Available online at [www.sciencedirect.com](http://www.sciencedirect.com)

## Damage in cement-based materials, studied by electrical resistance measurement

D.D.L. Chung\*

*Composite Materials Research Laboratory, University at Buffalo, State University of New York, Buffalo, NY 14260-4400, USA*

### Abstract

Real-time monitoring of a structural component gives information on the time and condition at which damage occurs, thereby facilitating the evaluation of the cause of the damage. Moreover, it provides information once damage occurs, thus enabling timely repair and hazard mitigation. Real-time monitoring also allows study of the damage evolution. This paper reviews the use of electrical resistance measurement to monitor damage in cement-based materials. This method is advantageous in its sensitivity to even minor, microscopic and reversible effects. Damage can occur within a cement-based material, at the interface between concrete and steel rebar, and at the interface between old concrete and new concrete (as encountered in the use of new concrete for repair of an old concrete structure). This paper addresses all three aspects of damage, whether the damage is due to static stress, dynamic stress, freeze–thaw cycling, creep or drying shrinkage. Moreover, monitoring during straining at various rates allows study of the effect of strain rate on the damage evolution.

© 2003 Elsevier B.V. All rights reserved.

*Keywords:* Cement; Concrete; Electrical resistance; Damage; Monitoring; Sensing

## 1. Damage monitoring

### 1.1. Technological need

The structural integrity of the civil infrastructure is essential for the safety, productivity and quality of life of the society. This integrity is often a concern due to the aging of the infrastructure, the occurrence of earthquakes, exposure to wind and ocean waves, soil movement, excessive loading, temperature excursions and terrorism. Thus, there is need for monitoring damage nondestructively, so that timely repair or retirement of structures takes place.

Damage sensing (i.e. structural health monitoring) is valuable for structures for the purpose of hazard mitigation. It can be conducted during the damage by acoustic emission detection. It can also be conducted after the damage by ultrasonic inspection, liquid penetrant inspection, dynamic mechanical testing or other techniques. Real-time monitoring gives information on the time, load condition or other conditions at which damage occurs, thereby facilitating the evaluation of the cause of the damage. Moreover, real-time monitoring provides information as soon as damage occurs, thus enabling timely repair or other hazard precaution measures.

\* Tel.: +1-716-645-2593x2243; fax: +1-716-645-3875.

*E-mail address:* [ddlchung@eng.buffalo.edu](mailto:ddlchung@eng.buffalo.edu) (D.D.L. Chung).

Real-time monitoring allows study of the damage evolution, which refers to how damage evolves in a damaging process and is the subject of much modeling work [1–12], due to its fundamental importance in relation to the science of damage. Limited experimental observation of the damage evolution has involved the use of acoustic emission [13–15], thermoelastic stress analysis [16] and computer tomography (CT) scanning [17]. In contrast, this paper uses electrical resistance measurement, which is advantageous in its sensitivity to even minor, microscopic and reversible effects. The ongoing challenge of the experimentalist is to relate such laboratory results to the structural integrity problems of the civil infrastructure.

Stress application can generate defects, which may be a form of damage in a material. Stress application can also heal defects, particularly in the case of the stress being compressive. This healing is induced by stress [18] and is to be distinguished from healing that is induced by liquids, chemicals or particles [19–29]. On the other hand, stress removal can aggravate defects, particularly in the case of the stress being compressive and the material being brittle. The generation, healing and aggravation of defects during dynamic loading are referred to as defect dynamics. The little prior attention on defect dynamics is mainly due to the dynamic nature of defect healing and aggravation. For example, stress application can cause healing, and subsequent unloading can cancel the healing. This reversible nature of the healing makes the healing observable only in real time during loading. On the other hand, defect generation tends to be irreversible upon unloading, so it does not require observation in real time.

Observation in real time during loading is difficult for microscopy, particularly transmission electron microscopy, which is the type of microscopy that is most suitable for the observation of microscopic defects. However, observation in real time during loading can be conveniently performed by electrical measurement. As defects usually increase the electrical resistivity of a material, defect generation tends to increase the resistivity whereas defect healing tends to decrease the resistivity.

The strain rate affects the damage evolution during static stress application, in addition to affecting the mechanical properties in the case of a viscoelastic material. Real-time monitoring by electrical resistivity measurement during straining at various rates allows study of the effect of strain rate on the damage evolution. Similarly, real-time electrical resistivity measurement allows monitoring of the damage evolution during creep, drying shrinkage, fatigue and freeze–thaw cycling.

## *1.2. Experimental methods*

Damage in cement-based materials is most commonly studied by destructive mechanical testing after different amounts of damage. However, this method does not allow the monitoring of the progress of damage on the same specimen and is not sufficiently sensitive to minor damage. As different specimens can differ in the flaws, damage evolution is more effectively studied by monitoring one specimen throughout the process rather than interrupting the process at different times for different specimens. However, the monitoring of one specimen throughout the process requires a nondestructive method that is sensitive to minor damage. Electrical resistivity measurement is effective for damage monitoring, particularly in the regime of minor damage, in addition to monitoring both defect generation and defect healing in real time.

The experimental method used throughout this paper is dc electrical resistance measurement, as conducted by using the four-probe method. In this method, the outer two electrical contacts are for passing current, whereas the inner two electrical contacts are for voltage measurement. Each electrical contact is made by using silver paint in conjunction with copper wire. The contacts are all on the specimen surface, rather than being embedded in the specimen. In the case of measuring the

volume resistance, each electrical contact is all the way around the specimen in a plane perpendicular to the direction of resistance measurement. The use of the two-probe method is unreliable, as the resistance associated with the electrical contacts is included in the measured resistance.

### 1.3. *Scope*

Damage sensing should be distinguished from strain sensing, as strain can be reversible and is not necessarily accompanied by damage. Damage can occur within a cement-based material, at the interface between concrete and steel rebar, at the interface between old concrete and new concrete (as encountered in the use of new concrete for repair of an old concrete structure), at the interface between unbonded concrete elements and at the interface between concrete and its carbon fiber–epoxy matrix composite retrofit. This paper addresses all these aspects of damage and is focused on the use of electrical resistance measurement for sensing damage, whether the damage is due to static stress, dynamic stress, freeze–thaw cycling, creep or drying shrinkage.

## 2. **Damage due to stress in a cement-based material**

This section covers the damage due to stress in a cement-based material that contain no fiber admixture and in one that contains an electrically conductive fiber admixture. The fiber enhances the damage sensing ability. In addition, it covers damage at the interface between concrete and steel rebar and the interface between new concrete and old concrete.

### 2.1. *Damage in a cement-based material without fibers*

This section covers the sensing of damage in cement paste, mortar and concrete, all without fibers. In addition, it covers the effect of strain rate on the damage evolution.

#### 2.1.1. *Cement paste*

Fig. 1 [30] shows the fractional change in longitudinal resistivity as well as the longitudinal strain during repeated compressive loading of plain cement paste at an increasing stress amplitude. The strain varies linearly with the stress up to the highest stress amplitude. The strain returns to zero at the end of each cycle of loading. During the first loading, the fractional change in resistivity increases due to defect generation. During the subsequent unloading, the fractional change in resistivity continues to increase, due to defect aggravation (such as the opening of the microcracks generated during prior loading). During the second loading, the resistivity decreases slightly as the stress increases up to the maximum stress of the first cycle (due to defect healing in the sense of reversibility of the measured resistance, i.e. a transient mechanical effect that is caused by pressure forcing contact to occur after a possibly chemical bond is broken through a brittle failure) and then increases as the stress increases beyond this value (due to additional defect generation). During unloading in the second cycle, the resistivity increases significantly (due to defect aggravation, probably the opening of the microcracks). During the third loading, the resistivity essentially does not change (or decreases very slightly) as the stress increases to the maximum stress of the third cycle (probably due to the balance between defect generation and defect healing). Subsequent unloading causes the resistivity to increase very significantly due to defect aggravation (probably the opening of the microcracks).

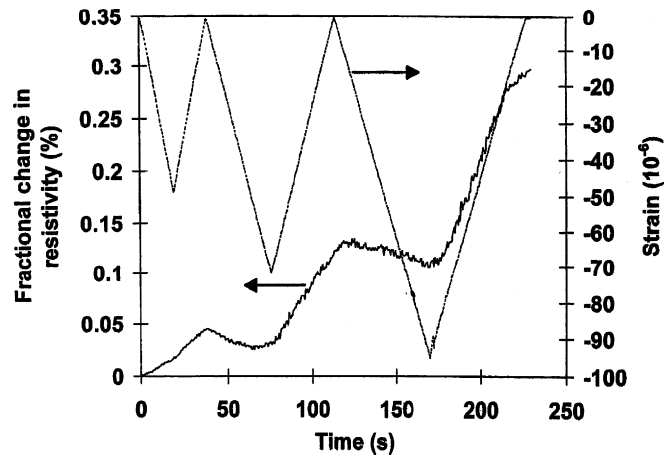


Fig. 1. Variation of the fractional change in electrical resistivity with time and of the strain (negative for compressive strain) with time during dynamic compressive loading at increasing stress amplitudes within the elastic regime for plain cement paste at 28 days of curing.

Fig. 2 [31] shows the fractional change in transverse resistivity as well as the transverse strain (positive due to the Poisson effect) during repeated compressive loading at an increasing stress amplitude. The strain varies linearly with the stress and returns to zero at the end of each cycle of loading. During the first loading and the first unloading, the resistivity increases due to defect generation and defect aggravation, respectively, as also shown by the longitudinal resistivity variation (Fig. 1). During the second loading, the resistivity first increases (due to defect generation) and then decreases (due to defect healing). During the second unloading, the resistivity increases due to defect aggravation. During the third loading, the resistivity decreases due to defect healing. During the third unloading, the resistivity increases due to defect aggravation.

The variations of the resistivity in the longitudinal and transverse directions upon repeated loading are consistent in showing defect generation (which dominates during the first loading), defect healing (which dominates during subsequent loading) and defect aggravation (which dominates during subsequent unloading). The defect aggravation during unloading follows the defect

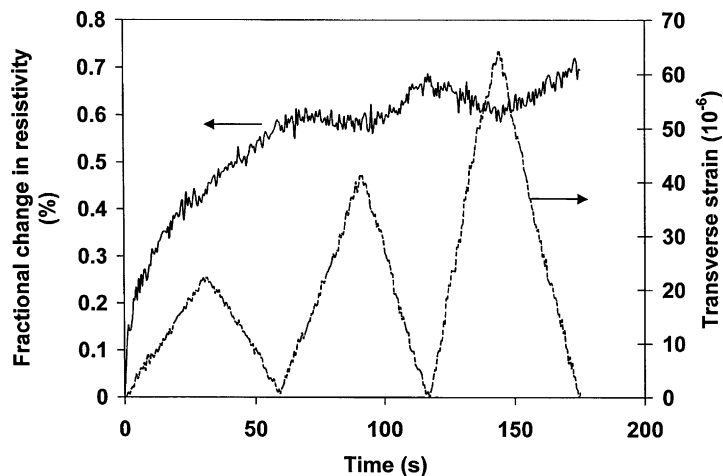


Fig. 2. Variation of the fractional change in transverse resistivity with time and of the transverse strain with time during dynamic compressive loading at increasing stress amplitudes within the elastic regime for plain cement paste.

healing during loading, indicating the reversible (not permanent) nature of the healing, which is induced by compressive stress. The defect aggravation during unloading also follows the defect generation during loading.

In spite of the Poisson effect, similar behavior was observed in the longitudinal and transverse resistivities. This means that these defects are essentially non-directional and that the resistivity variations are real.

Comparison of Figs. 1 and 2 shows that the increase in resistivity with strain during unloading in the second cycle is clearer and less noisy for the longitudinal resistivity than the transverse resistivity. This suggests that defect aggravation is more significantly revealed by the longitudinal resistivity than the transverse resistivity. Hence, the defects are not completely non-directional.

Identification of the defect type has not been made. Microcracks were mentioned earlier, just for the sake of illustration. The defects may be associated with certain heterogeneities in the cement paste.

Defects affect the mechanical properties. Therefore, mechanical testing (such as modulus measurement, which is nondestructive) can be used for studying defect dynamics. However, the modulus is not as sensitive to defect dynamics as the electrical resistivity; the relationship between stress and strain is not affected while the resistivity is affected. The low sensitivity of the modulus to defect dynamics is consistent with the fact that the deformation is elastic.

Fig. 3(a) [30] shows the fractional change in resistivity along the stress axis as well as the strain during repeated compressive loading at an increasing stress amplitude for plain cement paste. Fig. 3(b) shows the corresponding variation of stress and strain during the repeated loading. The strain varies linearly with the stress up to the highest stress amplitude (Fig. 3(b)). The strain does not return to zero at the end of each cycle of loading, indicating plastic deformation. In contrast, Figs. 1 and 2 are concerned with effects of elastic deformation.

The resistivity increases during loading and unloading in every loading cycle (Fig. 3(a)). The slope of the curve of resistivity versus time (Fig. 3(a)) increases with time, due to the increasing stress amplitude cycle by cycle (Fig. 3(b)) and the non-linear increase in damage severity as the stress amplitude increases. The resistivity increase during loading is attributed to damage infliction. The resistivity increase during unloading is attributed to the opening of microcracks generated during loading.

Fig. 4 [30] gives the corresponding plots for silica fume cement paste at the same stress amplitudes as Fig. 3. The strain does not return to zero at the end of each loading cycle, as in Fig. 3. The resistivity variation is similar to Fig. 3, except that the resistivity decreases during loading after the first cycle. The absence of a resistivity increase during loading after the first cycle is attributed to the lower tendency for damage infliction in the presence of silica fume, which is known to strengthen cement [31–34]. The resistivity decrease during loading after the first cycle is attributed to the partial closing of microcracks, as expected since the loading is compressive. In the absence of silica fume (i.e. plain cement paste, Fig. 3), the effect of damage infliction overshadows that of microcrack closing.

Fig. 5 [30] gives the corresponding plots for latex cement paste. The resistivity effects are similar to those of Fig. 4(a), except that the resistivity curve is less noisy and the rate of resistivity increase during first unloading is higher than that during first loading. This means that the microcrack opening during unloading has a larger effect on the resistivity than the damage infliction during loading.

Comparison of the results of Figs. 3–5 for deformation in the plastic regime with those of Figs. 1 and 2 for deformation in the elastic regime shows that both the fractional change in resistivity and the strain are higher in the plastic regime than in the elastic regime by orders of magnitude. Another difference is that the resistivity decreases are much less significant in the plastic regime than in the elastic regime. There is no resistivity decrease at all in Fig. 3(a), but there are resistivity decreases in Fig. 1. These differences between the results of plastic and elastic regimes are consistent with the

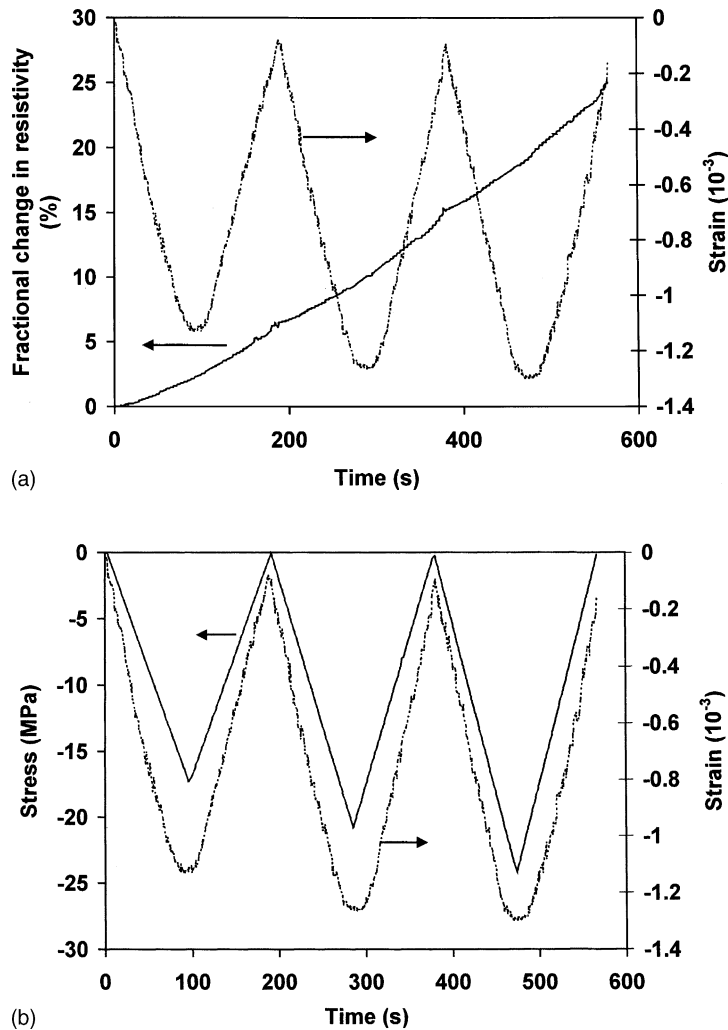


Fig. 3. Variation of the fractional change in electrical resistivity with time (a), of the stress with time (b), and of the strain (negative for compressive strain) with time ((a) and (b)) during dynamic compressive loading at increasing stress amplitudes for plain cement paste.

much greater damage in plastic deformation than in elastic deformation and the tendency of damage to increase the resistivity.

That the resistivity decreases are not significant in the plastic deformation regime simplifies the use of the electrical resistivity to indicate damage. Nevertheless, even when the resistivity decreases are significant, the resistivity remains a good indicator of damage, which includes that due to damage infliction (during loading) and that due to microcrack opening. Microcrack closing, which causes the resistivity decrease, is a type of partial healing, which diminishes the damage. Hence, the resistivity indicates both damage and healing effects in real time.

### 2.1.2. Mortars

Figs. 6 and 7 [30] show the variation of the fractional change in resistivity with cycle number during initial cyclic compression of plain mortar and silica fume mortar, respectively. For both mortars, the resistivity increases abruptly during the first loading (due to defect generation) and

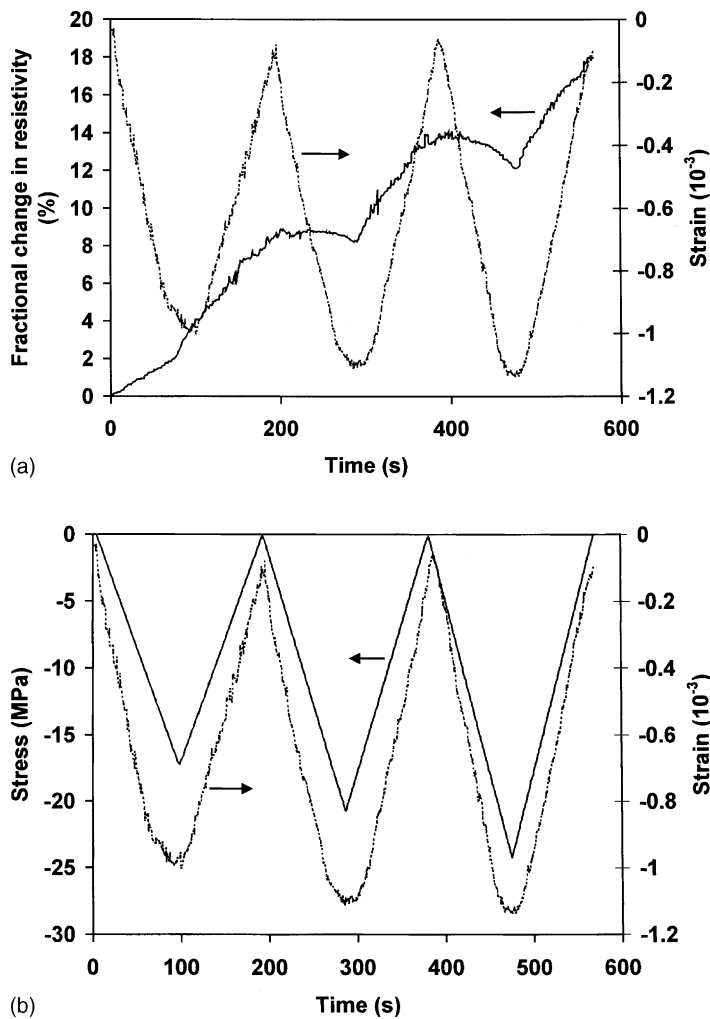


Fig. 4. Variation of the fractional change in electrical resistivity with time (a), of the stress with time (b), and of the strain (negative for compressive strain) with time ((a) and (b)) during dynamic compressive loading at increasing stress amplitudes for silica fume cement paste.

increases further during the first unloading (due to defect aggravation). Moreover, the resistivity decreases during subsequent loading (due to defect healing) and increases during subsequent unloading (due to defect aggravation); the effect associated with defect healing is much larger for silica fume mortar than for plain mortar. In addition, this effect intensifies as stress cycling at increasing stress amplitudes progresses for both mortars, probably due to the increase in the extent of minor damage. The increase in damage extent is also indicated by the resistivity baseline increasing gradually cycle by cycle. In spite of the increase in stress amplitude cycle by cycle, defect healing dominates over defect generation during loading in all cycles other than the first cycle.

Comparison of plain cement paste behavior (Section 2.1.1) and plain mortar behavior (this section) shows that the behavior is similar, except that the defect healing (i.e. the resistivity decrease upon loading other than the first loading) is much more significant in the mortar case. This means that the sand–cement interface in the mortar contributes significantly to the defect dynamics, particularly in relation to defect healing.

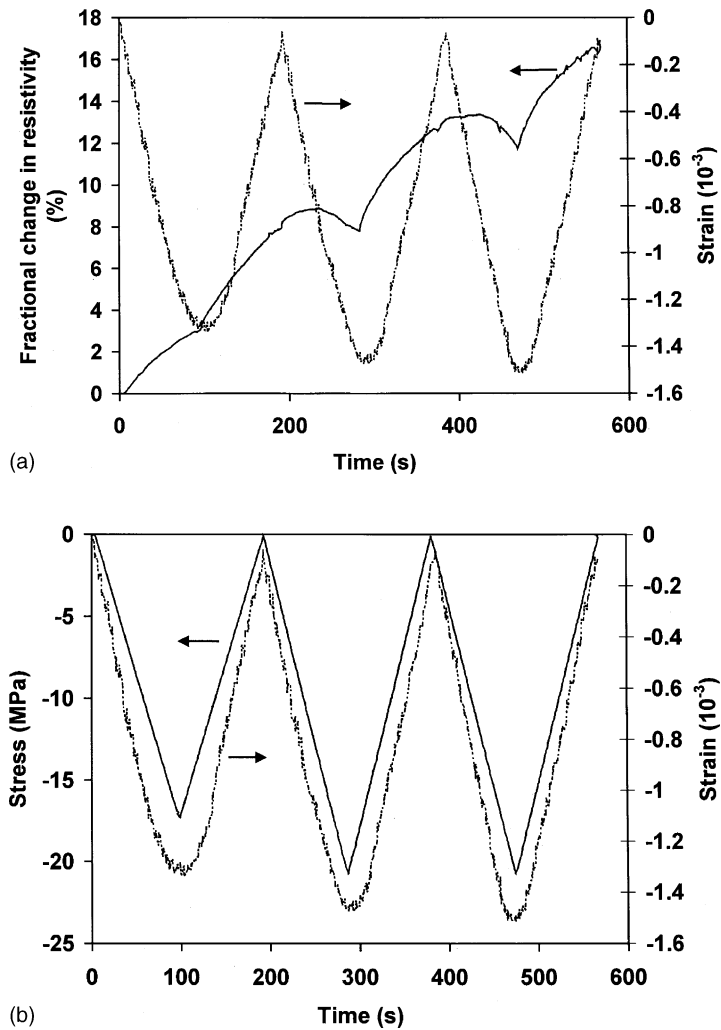


Fig. 5. Variation of the fractional change in electrical resistivity with time (a), of the stress with time (b), and of the strain (negative for compressive strain) with time ((a) and (b)) during dynamic compressive loading at increasing stress amplitudes for latex cement paste.

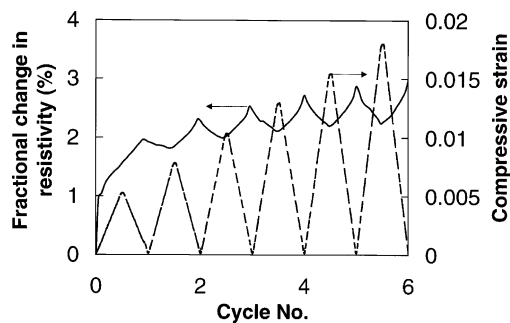


Fig. 6. Variation of the fractional change in resistivity with cycle number (thick curve) and of the compressive strain with cycle number (thin curve) during repeated compressive loading at increasing stress amplitudes within the elastic regime for plain mortar.

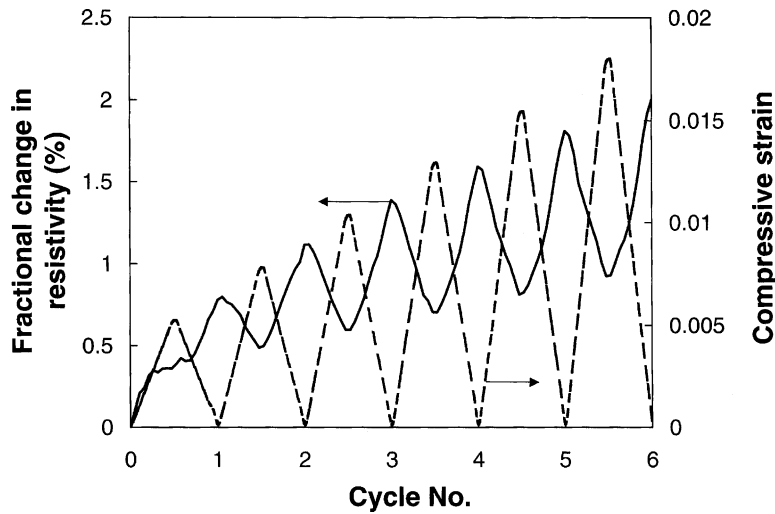


Fig. 7. Variation of the fractional change in resistivity with cycle number (thick curve) and of the compressive strain with cycle number (thin curve) during repeated compressive loading at increasing stress amplitudes within the elastic regime for silica fume mortar.

Comparison of Figs. 6 and 7 shows that silica fume contributes significantly to the defect dynamics. The associated defects are presumably at the interface between silica fume and cement, even though this interface is diffuse due to the pozzolanic nature of silica fume. The defects at this interface are smaller than those at the sand–cement interface, but this interface is large in total area due to the small size of silica fume compared to sand.

Figs. 8–10 [30] show the fractional change in resistivity in the stress direction versus cycle number during cyclic compression at a constant stress amplitude in the elastic regime (in contrast to the increasing stress amplitude in Figs. 6 and 7). Except for the first cycle, the resistivity decreases with increasing strain in each cycle and then increases upon subsequent unloading in the same cycle. As cycling progresses, the baseline resistivity continuously increases, such that the increase is quite abrupt in the first three cycles (Fig. 8) and that subsequent baseline increase is more gradual. In addition, as cycling progresses, the amplitude of resistivity decrease within a cycle gradually and continuously increases (Fig. 8).

The increase in baseline resistivity dominates the first cycle (Fig. 9) and corresponds to a fractional change in resistivity per longitudinal unit strain of  $-1.1$  (negative because the strain was negative). This negative value suggests that the baseline resistivity increase is due to damage

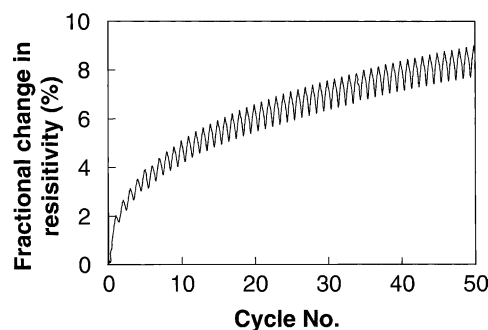


Fig. 8. Fractional change in resistivity and strain vs. compressive stress cycle number for cycles 1–50 for plain mortar.

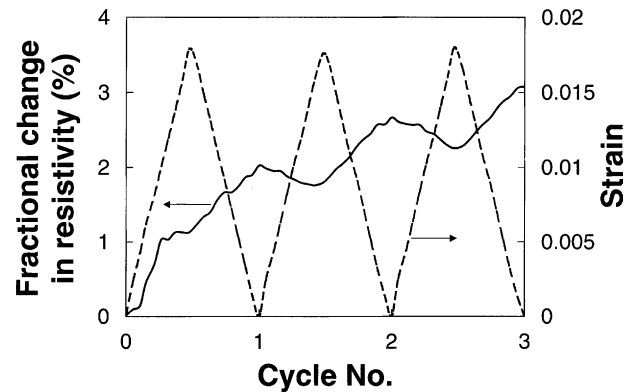


Fig. 9. Fractional change in resistivity and strain vs. compressive stress cycle number for cycles 1–3 for plain mortar.

(defect generation). The baseline resistivity increase is irreversible, indicating the irreversibility of the damage. The incremental increase in damage diminishes as cycling progresses, as shown by the baseline resistivity increasing more gradually as cycling progresses.

The reversible decrease in resistivity within a stress cycle corresponds to a fractional change in resistivity per unit strain of  $+0.72$  at cycle 50 (Fig. 10). It is attributed to defect healing (reversible) under the compressive stress. As cycling progresses, the cumulative damage (as indicated by the baseline resistivity) increases and results in a greater degree of defect healing upon compression (hence, more decrease in resistivity within a cycle).

Both the baseline resistivity and the amplitude of resistivity decrease within a cycle serve as indicators of the extent of damage. Measurement of the baseline resistance does not need to be done in real time during loading, thus simplifying the measurement. However, its use in practice is complicated by possible shifts in the baseline by environmental, polarization and other factors. On the other hand, the measurement of the amplitude of resistivity decrease must be done in real time during loading, but it is not much affected by baseline shifts.

The compressive strength before stress cycling is  $54.7 \pm 1.7$  MPa, and after 100 stress cycles is  $53.1 \pm 2.1$  MPa. The modulus, as shown by the change of strain with stress in each cycle, is not affected by the cycling. Thus, the damage that occurs during the stress cycling is slight, but is still detectable by resistivity measurement.

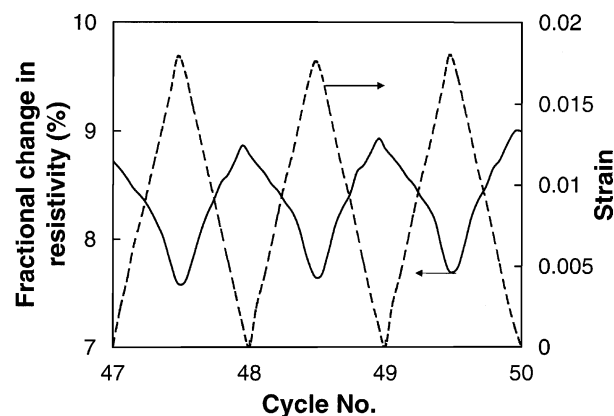


Fig. 10. Fractional change in resistivity and strain vs. compressive stress cycle number for cycles 48–50 for plain mortar.

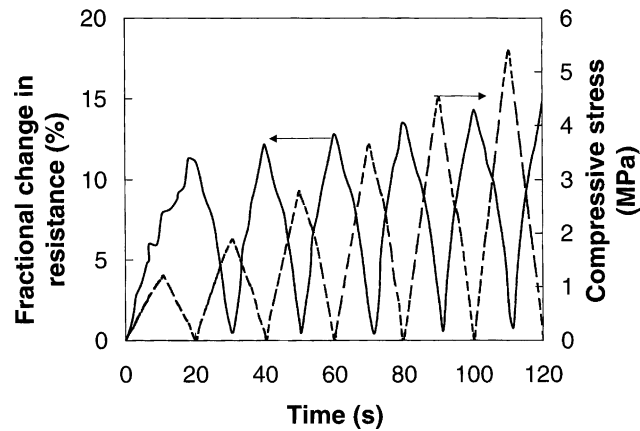


Fig. 11. Fractional change in resistance (solid curve) and stress (dashed curve) vs. time during repeated compressive loading at increasing stress amplitudes for plain concrete.

Comparison of the results of Section 2.1.1 on cement paste with those of this section on mortar shows that the fractional change in resistivity per unit strain (due to irreversible generation of defects in the elastic regime) is higher for mortar (1.10) than for cement paste (0.10). Moreover, comparison shows that mortar is more prone to defect healing (reversible) than cement paste, as expected from the presence of the interface between fine aggregate and cement in mortar.

### 2.1.3. Concrete

Fig. 11 [30] shows the fractional change in resistance in the stress direction during repeated compressive loading at increasing stress amplitudes. The resistance increases during loading and unloading in cycle 1, decreases during loading in all subsequent cycles and increases during unloading in all subsequent cycles. The higher the stress amplitude, the greater is the amplitude of resistance variation within a cycle.

The increase in resistance during loading in cycle 1 is attributed to defect generation; that during subsequent unloading in cycle 1 is attributed to defect aggravation. In all subsequent cycles, the decrease in resistance during loading is attributed to defect healing and the increase in resistance during unloading is attributed to defect aggravation.

The results of this section on concrete are consistent with those of Section 2.1.2 on mortar and those of Section 2.1.1 on cement paste. The compressive strength is higher for mortar than concrete. The defect dynamics, as indicated by the fractional change in resistance within a cycle, are more significant for concrete than mortar. The first healing, as indicated by the resistance decrease during loading in cycle 2, is much more complete for concrete than mortar. These observations mean that the interface between mortar and coarse aggregate contributes to the defect dynamics (particularly healing), due to the interfacial voids and defects.

Figs. 12–14 [30] show the fractional change in resistance in the stress direction versus cycle number during cyclic compression at a constant stress amplitude. Except for the first cycle, the resistance decreases with increasing stress in each cycle and then increases upon subsequent unloading in the same cycle. As cycling progresses, the baseline resistivity gradually and irreversibly increases (Fig. 12). In addition, as cycling progresses, the amplitude of resistance decrease within a cycle gradually and continuously increases, especially in cycles 1–9 (Fig. 12).

In the first cycle, the resistance increases upon loading and unloading, in contrast to all subsequent cycles, where the resistance decreases upon loading and increases upon unloading (Fig. 13).

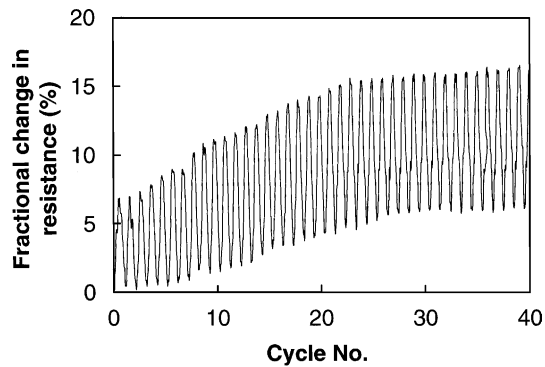


Fig. 12. Fractional change in resistance vs. compressive stress cycle number for cycles 1–40 for plain concrete.

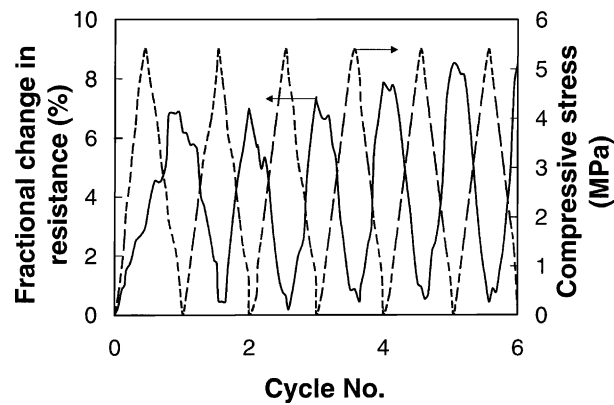


Fig. 13. Fractional change in resistance (solid curve) and stress (dashed curve) vs. compressive stress cycle number for cycles 1–6 for plain concrete.

The compressive strength before stress cycling is  $16.73 \pm 0.86$  MPa, and after 40 stress cycles is  $14.24 \pm 0.97$  MPa. Thus, the damage that occurs during the stress cycling is slight, but is still detectable by resistance measurement.

The gradual increase in baseline resistance as stress cycling progressed (Fig. 12) is attributed to irreversible and slight damage. The increase in the amplitude of resistance variation as cycling progresses (Fig. 12) is attributed to the effect of damage on the extent of defect dynamics. In other

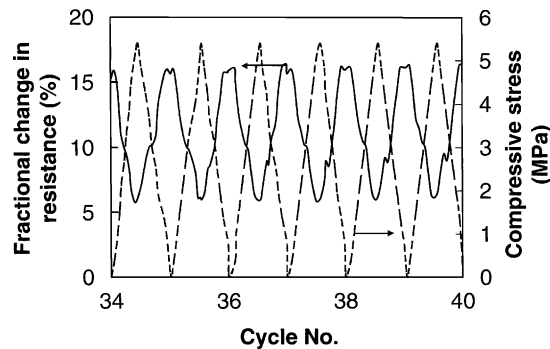


Fig. 14. Fractional change in resistance (solid curve) and stress (dashed curve) vs. compressive stress cycle number for cycles 35–40 for plain concrete.

words, the more is the damage, the greater is the extent of defect healing during loading and the greater is the extent of defect aggravation during unloading.

The fractional loss in compressive strength after the cycling is greater for concrete than mortar, as expected from the higher compressive strength of mortar. Nevertheless, the baseline resistance increase is more significant for mortar than concrete, probably due to the relatively large area of the interface between cement and fine aggregate and the consequent greater sensitivity of the baseline resistivity to the quality of the interface between cement and fine aggregate than to the quality of the interface between mortar and coarse aggregate. In other words, the interface between cement and fine aggregate dominates the irreversible electrical effects.

#### 2.1.4. Effect of strain rate

The mechanical properties of cement-based material are strain rate sensitive. As for most materials (whether cement-based or not), the measured strength (whether tensile or compressive) increases with increasing strain rate [35]. This effect is practically important due to the high strain rate encountered in earthquakes and in impact loading. The effect is less for high strength concrete than normal concrete [36] and is less at a curing age of 28 days than at an early age [37]. The cause of the effect is not completely understood, although it is related to the effect of strain rate on the crack propagation [35,38–40].

Although fracture mechanics [36,41,42], failure analysis [38] and mechanical testing over a wide range of strain rate [38,43,44] have been used to study the phenomenon and cause of the strain rate sensitivity of cement-based materials, the current level of understanding is limited. This is partly because of the experimental difficulty of monitoring the microstructural change during loading. Observation during loading is in contrast to that after loading. The former gives information on the damage evolution, whether the latter does not. Work on observation during loading is mainly limited to determination of the stress–strain relationship during loading. Although this relationship is important and basic, it does not give microstructural information. The use of a nondestructive real-time monitoring technique during loading is desirable. Microscopy is commonly used for microstructural observation, but it is usually not sensitive to subtle microstructural changes in a cement-based material and is not suitable for real-time monitoring. On the other hand, electrical resistivity measurement is nondestructive and fast.

Fig. 15 [45] shows the fractional change in resistivity in the stress direction versus the strain in the stress direction during compressive testing up to failure of cement mortar (without fiber) at three different loading rates. The resistivity increases monotonically with strain and stress, such that the resistivity increase is most significant when the strain or stress is low compared to the strain or stress at fracture. Similar curvature of the resistivity curve (Fig. 15) occurs for all three loading rates. At fracture, the resistivity abruptly increases, as expected. Fig. 16 [45] shows the stress versus strain at different loading rates. The stress–strain curve is a straight line up to failure for any of the loading rates, indicating the brittleness of the failure. The higher the loading rate, the lower is the fractional change in resistivity at fracture and the higher is the compressive strength, as shown in Table 1.

Table 1  
Effect of strain rate on the compressive properties of mortar (without fiber)

Loading rate (MPa s <sup>-1</sup> )	Strain rate (10 <sup>-5</sup> s <sup>-1</sup> )	Strength (MPa)	Modulus (GPa)	Ductility (%)	Fractional change in resistivity at fracture
0.144	5.3	41.4 ± 1.6	1.83 ± 0.17	1.9 ± 0.2	1.78 ± 0.24
0.216	8.8	43.2 ± 1.0	1.85 ± 0.14	1.8 ± 0.2	1.10 ± 0.13
0.575	23.3	45.7 ± 2.1	1.93 ± 0.17	1.8 ± 0.3	0.81 ± 0.16

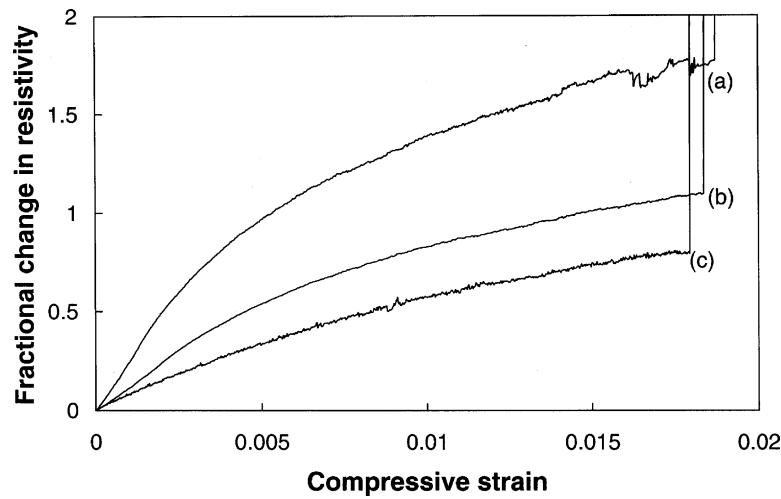


Fig. 15. Fractional change in resistivity vs. strain during compressive testing up to failure of mortar (without fiber) at loading rates of: (a)  $0.144 \text{ MPa s}^{-1}$ ; (b)  $0.216 \text{ MPa s}^{-1}$ ; (c)  $0.575 \text{ MPa s}^{-1}$ .

The modulus and ductility essentially do not vary with the loading rate in the range of loading rate used, although the modulus slightly increases and the ductility slightly decreases with increasing loading rate, as expected.

The electrical resistivity is a geometry-independent property of a material. The gradual resistivity increase observed at any of the loading rates as the stress/strain increases indicates the occurrence of a continuous microstructural change, which involves the generation of defects that cause the resistivity to increase. The microstructural change is most significant in the early part of the loading. At any strain, the extent of microstructural change, as indicated by the fractional change in resistivity, decreases with increasing loading rate. In addition, the amount of damage at failure, as indicated by the fractional change in resistivity at failure, decreases with increasing strain rate. Hence, the loading rate affects not only the failure conditions, but also the damage evolution, all the

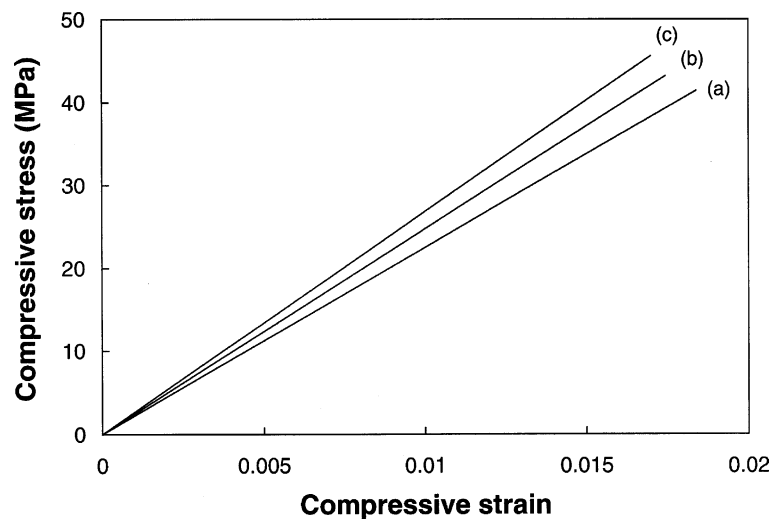


Fig. 16. Stress vs. strain during compressive testing up to failure of mortar (without fiber) at loading rates of: (a)  $0.144 \text{ MPa s}^{-1}$ ; (b)  $0.216 \text{ MPa s}^{-1}$ ; (c)  $0.575 \text{ MPa s}^{-1}$ .

way from the early part of the loading. A higher loading rate results in less time for microstructural changes, thereby leading to less damage build-up. The loading rate will likely also affect the populations of the various types of defects generated, but investigation of defect types and their populations requires techniques other than electrical resistance measurement. Examples of other techniques are environmental scanning tunneling microscopy, small angle neutron scattering, positron annihilation and synchrotron X-ray scattering. However, none of these techniques has been used for the monitoring of cement-based materials.

## 2.2. Sensing damage in a cement-based material containing conductive short fibers

In short fiber-reinforced concrete, the bridging of the cracks by fibers limits the crack height to values much smaller than those of concretes without fiber reinforcement. For example, the crack height is less than 1  $\mu\text{m}$  in carbon fiber-reinforced mortar after compression to 70% of the compressive strength, but is about 100  $\mu\text{m}$  in mortar without fibers after compression to 70% of the corresponding compressive strength (Fig. 6 of [46]). As a result, the regime of minor damage is more dominant when fibers are present.

Cement reinforced with short carbon fibers is attractive due to its high flexural strength and toughness and low drying shrinkage, in addition to its strain sensing ability. The strain sensing ability stems from the effect of strain on the microcrack height and the consequent slight pull-out or push-in of the fiber that bridges the crack [46]. Fiber pull-out occurs during tensile strain and causes an increase in the contact electrical resistivity at the fiber–matrix interface, thereby increasing the volume resistivity of the composite. Fiber push-in occurs during compressive strain and causes a decrease in the volume resistivity of the composite [46].

While reversible changes in electrical resistance upon dynamic loading relates to dynamic strain, irreversible changes in resistance relate to damage. The resistance of carbon fiber-reinforced cement mortar decreases irreversibly during the early stage of fatigue (the first 10% or less of the fatigue life) due to matrix damage resulting from multiple cycles of fiber pull-out and push-in [47]. The matrix damage enhances the chance of adjacent fibers to touch one another, thereby decreasing the resistivity. Beyond the early stage of fatigue and up to the end of the fatigue life, there is no irreversible resistance change, other than the abrupt resistance increase at fracture [47]. The absence of an irreversible change before fracture indicates that the mortar is not a good sensor of its fatigue damage.

Fatigue damage is to be distinguished from damage under increasing stresses. The former typically involves stress cycling at a low stress amplitude [47], whereas the latter typically involves higher stresses. The former tends to occur more gradually than the latter. Thus, the failure to sense fatigue damage [47] does not suggest failure to sense damage, in general.

The sensing of damage under increasing stresses has been demonstrated in carbon fiber-reinforced concrete [48] and carbon fiber-reinforced mortar [49]. The damage is accompanied by a partially reversible increase in the electrical resistivity of the concrete. The greater the damage, the larger is the resistivity increase. As fiber breakage would have resulted in an irreversible resistivity increase, the damage is probably not due to fiber breakage, but due to partially reversible interface degradation. The interface could be that between fiber and matrix. Damage was observed within the elastic regime, even in the absence of a change in modulus.

Carbon fiber-reinforced concrete can monitor both strain and damage simultaneously through electrical resistance measurement. The resistance decreases upon compressive strain and increases upon damage. This means that the stress/strain condition (during dynamic loading) under which damage occurs can be obtained, thus facilitating damage origin identification.

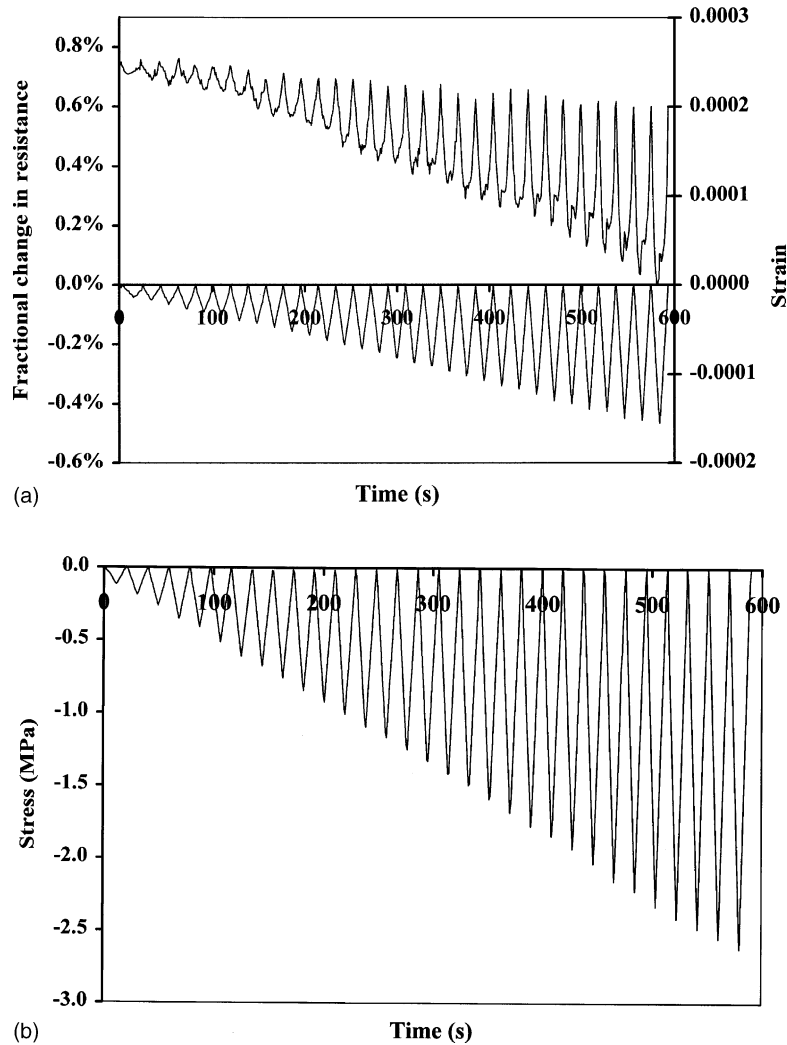


Fig. 17. Fractional change in resistance (upper curve in (a)), strain (lower curve in (a)) and stress (b) during repeated compressive loading of carbon fiber-reinforced concrete at increasing stress amplitudes up to 20% of the compressive strength.

Fig. 17 [48] shows the fractional change in resistance, strain and stress during repeated compressive loading of carbon fiber (2 wt.% of cement) reinforced concrete at increasing stress amplitudes up to 20% of the compressive strength (within the elastic regime) [48]. The strain returns to zero at the end of each loading cycle. The resistance decreases reversibly upon loading in each cycle. The higher the stress amplitude, the greater is the extent of resistance decrease. As load cycling progresses, the resistance at zero load decreases gradually cycle by cycle. In addition, an extra peak in the resistance curve appears after the first 16 cycles in Fig. 17 and becomes larger and larger as cycling progresses. The maximum of the extra peak occurs at the maximum stress of the cycle.

Fig. 18 [48] shows the fractional change in resistance, strain and stress during repeated compressive loading at increasing and decreasing stress amplitudes. The highest stress amplitude is 40% of the compressive strength. A group of cycles in which the stress amplitude increased cycle by cycle and then decreased cycle by cycle back to the initial low stress amplitude is hereby referred to

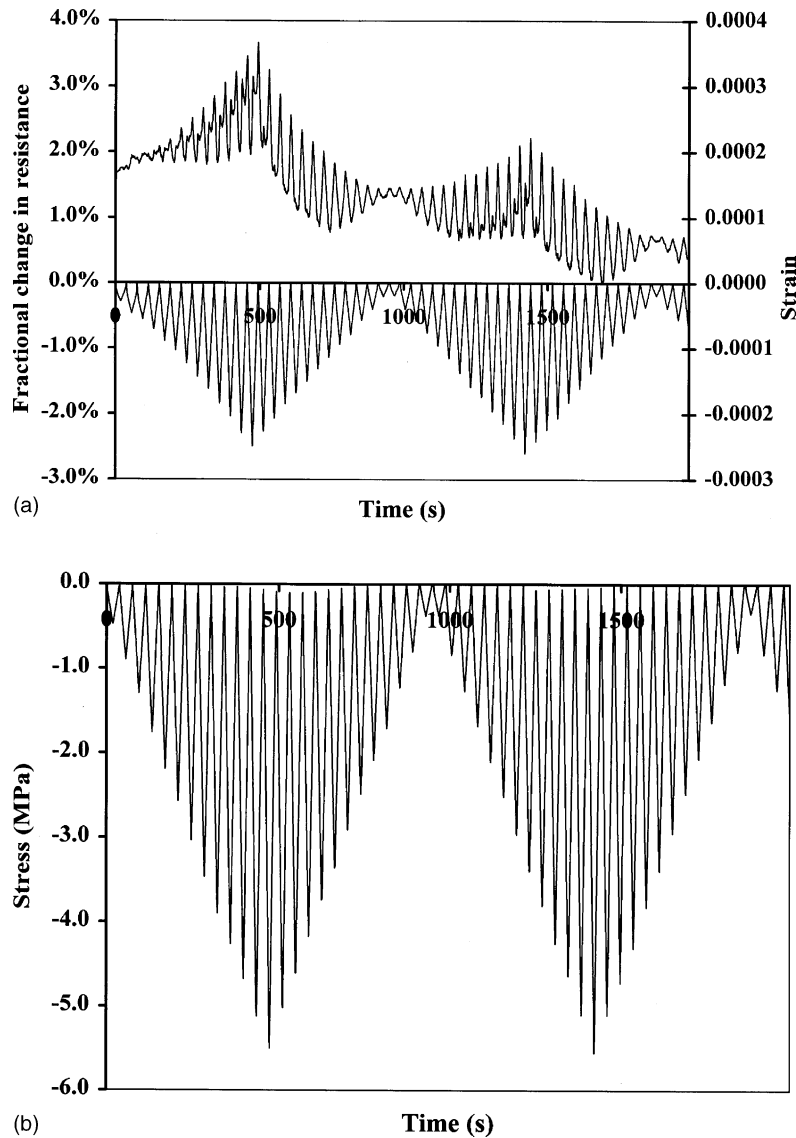


Fig. 18. Fractional change in resistance (upper curve in (a)), strain (lower curve in (a)) and stress (b) during repeated compressive loading of carbon fiber-reinforced concrete at increasing and decreasing stress amplitudes, the highest of which was 40% of the compressive strength.

as a group. Fig. 18 [48] shows the results for two groups, plus the beginning of the third group. The strain returns to zero at the end of each cycle for any of the stress amplitudes, indicating elastic behavior. Fig. 19 [48] shows a magnified view of the first half of the first group. The resistance decreases upon loading in each cycle, as in Fig. 17. The extra peak at the maximum stress of a cycle grows as the stress amplitude increases, as in Fig. 17. However, in contrast to Fig. 18, the extra peak quickly becomes quite large, due to the higher maximum stress amplitude in Fig. 18 than in Fig. 17. In Fig. 18, there are two peaks per cycle. The original peak (larger peak) occurs at zero stress, while the extra peak (smaller peak) occurs at the maximum stress. Hence, during loading from zero stress within a cycle, the resistance drops and then increases sharply, reaching the maximum resistance of the extra peak at the maximum stress of the cycle. Upon subsequent unloading, the resistance

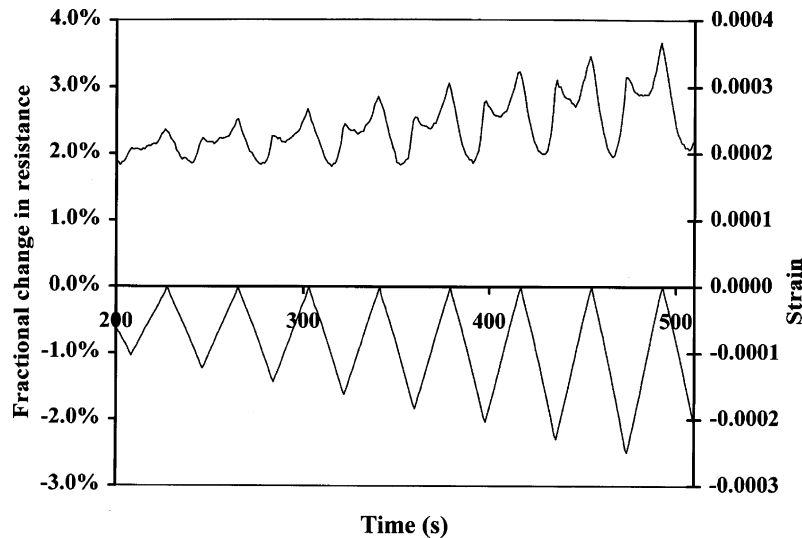


Fig. 19. A magnified view of the first 500 s of Fig. 18(a).

decreases and then increases as unloading continues, reaching the maximum resistance of the original peak at zero stress. In the part of this group where the stress amplitude decreases cycle by cycle, the extra peak diminishes and disappears, leaving the original peak as the sole peak. In the part of the second group where the stress amplitude increases cycle by cycle, the original peak (peak at zero stress) is the sole peak, except that the extra peak (peak at the maximum stress) returns in a minor way (more minor than in the first group) as the stress amplitude increases. The extra peak grows as the stress amplitude increases, but, in the part of the second group in which the stress amplitude decreases cycle by cycle, it quickly diminishes and vanishes, as in the first group. Within each group, the amplitude of resistance variation increases as the stress amplitude increases and decreases as the stress amplitude subsequently decreases. The baseline resistance decreases gradually from the first group to the second group.

Fig. 18(b) [48] shows similar results for three successive groups with the highest stress amplitude being 60% of the compressive strength. As the stress amplitude increases, the extra peak at the maximum stress of a cycle grows to the extent that it is comparable to the original peak at zero stress. The decrease of the baseline resistance from group to group is negligible, in contrast to Fig. 18(a). Other features of Fig. 18(a) and (b) are similar.

Fig. 20 [48] shows four successive groups and the beginning of the fifth group, with the highest stress amplitude being more than 90% of the compressive strength. The highest stress amplitude is the same for each group (Fig. 20(b)), but the highest strain amplitude of a group increases from group to group as load cycling progresses (Fig. 20(a)). In contrast, the highest strain amplitude of a group does not change from group to group in Fig. 20(b). This means that the modulus decreases as cycling occurs in Fig. 20(a), whereas the modulus does not change in Fig. 20(b). In Fig. 20, the resistance increases in every cycle. The extra peak at the maximum stress of a cycle is the sole peak in each cycle. The original peak at zero stress does not appear at all. In each group, the amplitude of resistance change in a cycle increases with increasing stress amplitude and subsequently decreases with decreasing stress amplitude. In each group, the resistance increases abruptly as the maximum stress amplitude of the group is about to be reached. The baseline resistance increases gradually from group to group.

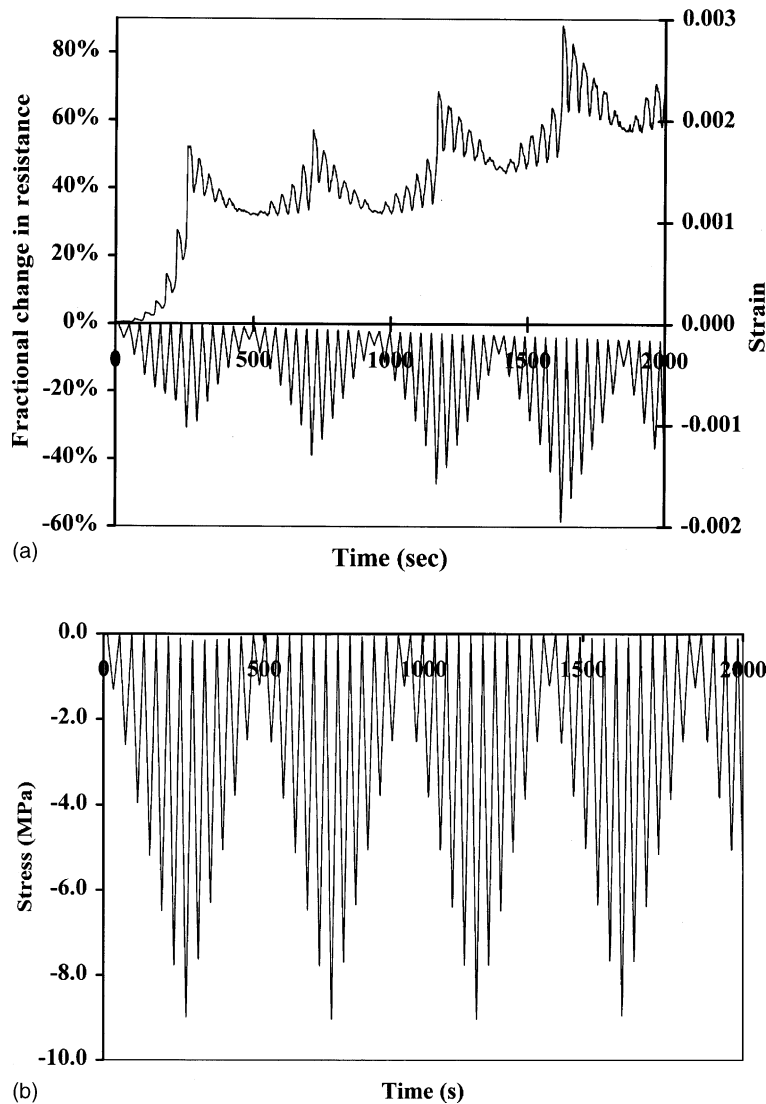


Fig. 20. Fractional change in resistance (upper curve in (a)), strain (lower curve in (a)) and stress (b) during repeated compressive loading of carbon fiber-reinforced concrete at increasing and decreasing stress amplitudes, the highest of which was >90% of the compressive strength.

Fig. 21 [48] shows the results for loading in which the stress amplitude increases cycle by cycle to a maximum (more than 90% of the compressive strength) and is held at the maximum for numerous cycles (Fig. 21(b)). The strain amplitude (Fig. 21(a)) increases along with the stress amplitude, but continues to increase after the stress amplitude has reached its maximum. This indicates a continuous decrease in modulus after the maximum stress amplitude has been reached. The resistance increases as the stress increases in each cycle, as in Fig. 20. The baseline resistance increases significantly cycle by cycle and continues to increase after the stress amplitude has reached its maximum.

Carbon fiber-reinforced concrete is able to sense its own damage, which occurs under increasing stress even within the elastic regime. The damage is partially reversible, as indicated by the partially reversible increase in electrical resistivity observed during cyclic loading at a stress

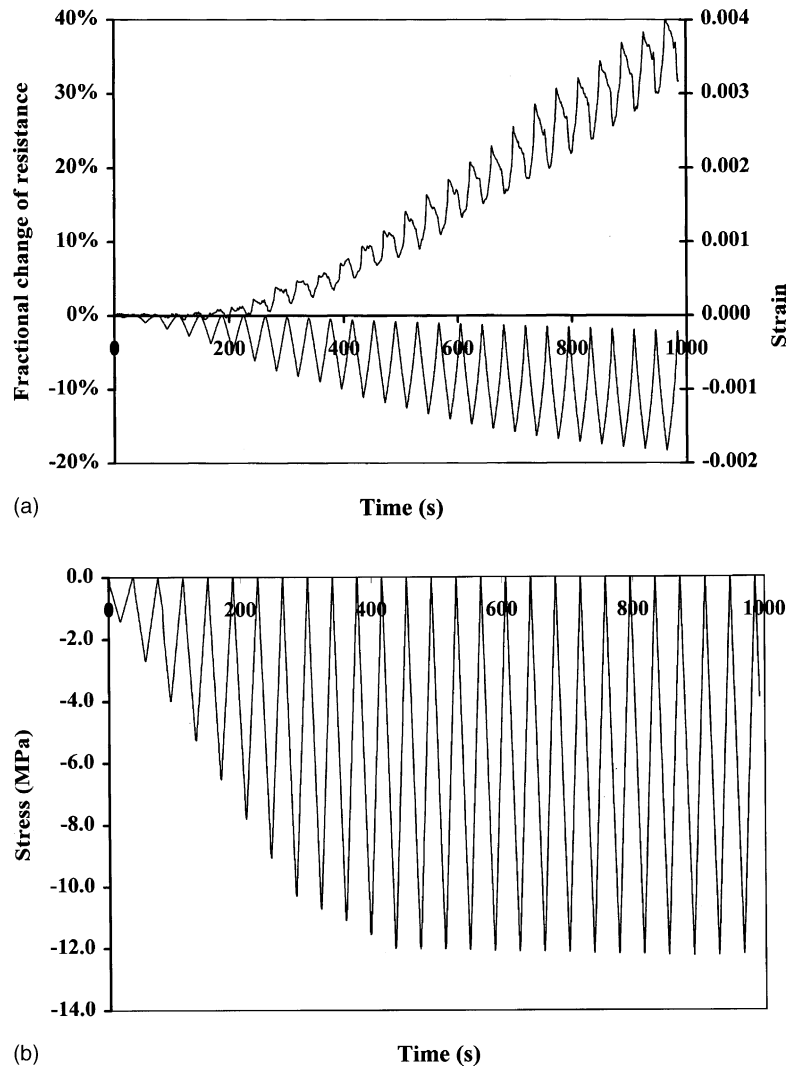


Fig. 21. Fractional change in resistance (upper curve in (a)), strain (lower curve in (a)) and stress (b) during repeated compressive loading of carbon fiber-reinforced concrete at increasing stress amplitudes up to >90% of the compressive strength and then with the stress amplitude fixed at the maximum.

amplitude which increases cycle by cycle. In contrast, compressive strain is indicated by a reversible decrease in resistivity. Upon increasing the stress, the group in which the stress amplitude increases cycle by cycle. This resistance increase indicates the occurrence of damage. Upon decreasing the stress amplitude, the extra peak does not occur, except for the first two cycles of stress amplitude decrease. The greater the stress amplitude, the larger and the less reversible is the damage-induced resistance increase (the extra peak). The resistance starts to increase at a stress higher than that in prior cycles and continues to increase until the stress reaches the maximum in the cycle, thereby resulting in the extra peak at the maximum stress of a cycle in the part of a partial irreversibility is clearly shown in Figs. 20 and 21. If the stress amplitude has been experienced before, the damage-induced resistance increase (the extra peak) is small, as shown by comparing the result of the second group with that of the first group (Figs. 18 and 19), unless the extent of damage is large (Figs. 20 and 21). When the damage is extensive (as shown by a modulus decrease), damage-induced resistance

increase occurs in every cycle (Fig. 20), even at a fixed stress amplitude (Fig. 21) or at a decreasing stress amplitude (Fig. 20), and it can overshadow the strain-induced resistance decrease (Figs. 20 and 21). Hence, the damage-induced resistance increase occurs mainly during loading (even within the elastic regime), particularly at a stress above that in prior cycles, unless the stress amplitude is high and/or damage is extensive.

At a low stress amplitude, the baseline resistance decreases irreversibly and gradually cycle by cycle (Figs. 17 and 18). This is the same as the effect [46] attributed to matrix damage and consequent enhancement of the chance of adjacent fibers to touch one another. At a high stress amplitude, this baseline resistance decrease is overshadowed by the damage-induced resistance increase, the occurrence of which cycle by cycle as the stress amplitude increases causes the baseline resistance to increase irreversibly (Figs. 20 and 21). These two opposing baseline effects cause the baseline to remain flat at an intermediate stress amplitude (Fig. 21).

The baseline resistance in the regime of major damage (with a decrease in modulus) provides a measure of the extent of damage (i.e. condition monitoring). This measure works in the loaded or unloaded state. In contrast, the measure using the damage-induced resistance increase works only during stress increase and indicates the occurrence of damage (whether minor or major) as well as the extent of damage.

The damage causing the partially reversible damage-induced resistance increase is probably mainly associated with partially reversible degradation of the fiber–matrix interface. The reversibility rules out fiber fracture as the main type of damage, especially at a low stress amplitude. At a high stress amplitude, the extent of reversibility diminishes and fiber fracture may contribute to causing the damage. Fiber fracture can occur during the opening of a crack that is bridged by a fiber. The fiber–matrix interface degradation may be associated with slight fiber pull-out upon slight crack opening for cracks that are bridged by fibers. The severity of the damage-induced resistance increase supports the involvement of the fibers in the damage mechanism, as the fibers are much more conducting than the matrix.

In the regime of elastic deformation, the damage does not affect the strain permanently, as shown by the total reversibility of the strain during cyclic loading (Figs. 17–21). Nevertheless, damage occurs during stress increase, as shown by the damage-induced resistance increase. Damage occurs even in the absence of a change in modulus. Hence, the damage-induced resistance increase is a sensitive indicator of minor damage (without a change in modulus), in addition to being a sensitive indicator of major damage (with a decrease in modulus). In contrast, the baseline resistance increase is an indicator of major damage only.

### *2.3. Damage at the interface between concrete and steel rebar*

Steel reinforced concrete is a widely used structural material. The effectiveness of the steel reinforcement depends on the bond between the steel reinforcing bar (rebar) and the concrete. Destructive measurement of the shear bond strength by pull-out, push-in and related testing methods is commonly used to assess the quality of the bond [50–64]. Nondestructive methods of bond assessment are attractive for condition evaluation in the field. They include acoustic [65–67] and electrical [68] methods. In particular, measurement of the contact electrical resistivity of the bond interface has been used to investigate the effects of admixtures, water/cement ratio, curing age, rebar surface treatment and corrosion on the steel–concrete bond [68]. This electrical method can be used to monitor in real time the degradation of the bond during cyclic shear loading [69]. Cyclic loading may lead to fatigue and the damage evolution is of scientific and technological interest.

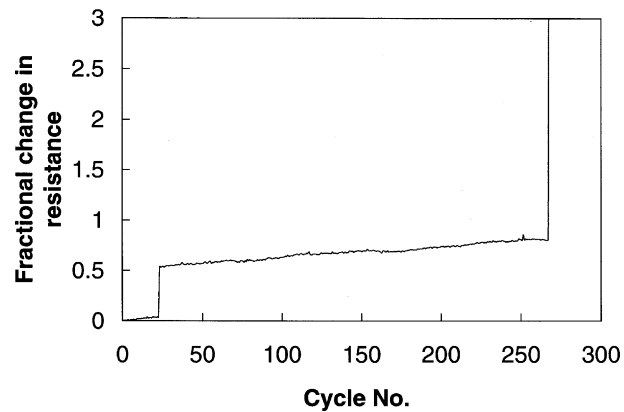


Fig. 22. Variation of the fractional contact resistance change with cycle number during cyclic shear loading at a shear stress amplitude of 3.73 MPa up to bond failure. The contact resistance is that of the interface between concrete and steel rebar.

Fig. 22 [69] shows the fractional change in contact electrical resistance of the joint between steel and concrete during cyclic shear loading at a shear stress amplitude of 3.73 MPa. The resistance does not change much upon stress cycling except for an abrupt increase after 8–31 cycles (the particular cycle depending on the sample), when there is no visual sign of damage, and another abrupt increase at bond failure, which occurs at cycles 220–270 (the particular cycle depending on the sample).

Fig. 23 [69] shows the fractional change in contact electrical resistance during cyclic shear loading at a shear stress amplitude of 0.75 MPa. The resistance abruptly increases after 150–210 cycles (depending on the sample), due to bond degradation, which is not visually observable. Bond failure does not occur up to 400 cycles, at which testing is stopped. The bond strength before any cyclic shear is  $6.68 \pm 0.24$  MPa, and after the abrupt increase (at the end of 400 cycles in Fig. 23) is  $5.54 \pm 0.43$  MPa. Thus, even though the abrupt increase does not cause visually observable damage, bond degradation occurs.

Comparison of Figs. 22 and 23 shows that a higher stress amplitude causes bond degradation and bond failure to occur at lower number of cycles, as expected. The abrupt increase in resistance due to bond degradation (not bond failure) (Figs. 22 and 23) provides a method of monitoring bond quality nondestructively in real time during dynamic loading. In contrast, bond strength measurement by mechanical testing is destructive. The bond degradation is attributed to fatigue.

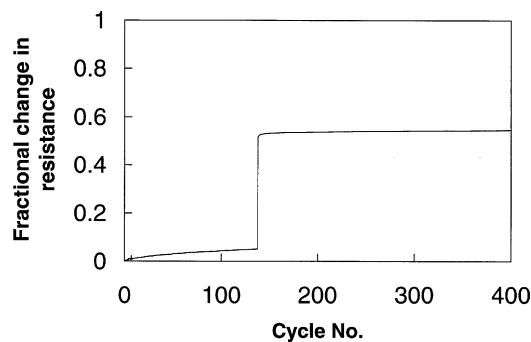


Fig. 23. Variation of the fractional contact resistance change with cycle number during cyclic shear loading at a shear stress amplitude of 0.75 MPa. The test was stopped prior to bond failure. The contact resistance is that of the interface between concrete and steel rebar.

#### 2.4. Damage at the interface between new concrete and old concrete

The repair of a concrete structure commonly involves the bonding of new concrete to the old concrete [65–76]. Partly due to the drying shrinkage of the new concrete, the quality of the bond is limited. Destructive measurement of the shear bond strength has been previously used to assess the quality of the bond [77]. However, the bond may degrade at stresses below the shear bond strength, even though the degradation may not be visible. This degradation may occur during static or cyclic loading. In particular, cyclic loading may lead to fatigue. Such degradation is revealed by measurement of the contact electrical resistance of the bond interface during cyclic shear loading, as degradation causes the contact resistance to increase [78].

Measurement of the contact electrical resistance between old and new mortars has also been previously used to assess the performance of carbon fiber-reinforced mortar as an electrical contact material for cathodic protection [79]. However, the measurement was not carried out during mechanical loading.

Fig. 24 [78] shows the fractional change in contact electrical resistance of the joint between old and new mortars during cyclic shear loading at a shear stress amplitude of 1.21 MPa. The resistance does not change upon stress cycling except for an abrupt increase after 1–6 cycles (the particular cycle depending on the sample), when there is no visual sign of damage, and another abrupt increase at bond failure, which occurs at cycles 18–27 (the particular cycle depending on the sample).

The bond strength before the first abrupt increase is  $2.87 \pm 0.18$  MPa, and after the first abrupt increase is  $2.38 \pm 0.22$  MPa. Thus, even though the first abrupt increase does not cause visually observable damage, bond degradation occurs.

During static loading, the contact resistance increases monotonically with increasing shear stress and abruptly increases at bond failure, as shown in Fig. 25 [78] for the case of a specimen which has not been loaded prior to the measurement. No abrupt increase in resistance occurs during static loading prior to failure, in contrast to the observation of an abrupt increase prior to fatigue failure (Fig. 24).

Fig. 26 [78] shows the fractional change in contact electrical resistance during cyclic shear loading at a shear stress amplitude of 0.97 MPa (lower than that of Fig. 24). The resistance shows the

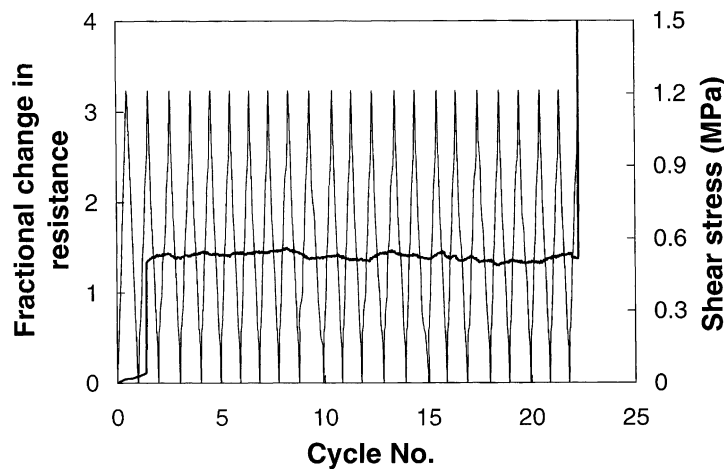


Fig. 24. Variation of the fractional contact resistance change with cycle number during cyclic shear loading of a joint between old and new mortars at a shear stress amplitude of 1.21 MPa up to bond failure. Thick curve: fractional change in contact resistance. Thin curve: shear stress. The contact resistance is that of the interface between old and new mortars.

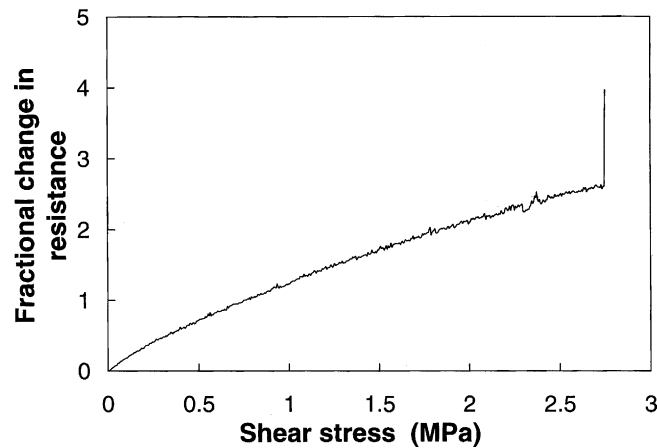


Fig. 25. Variation of the fractional contact resistance change with shear stress during static shear loading of a joint between old and new mortars up to failure. The contact resistance is that of the interface between old and new mortars.

first abrupt increase after 22–48 cycles (the particular cycle depending on the sample), and another abrupt increase at bond failure, which occurs after 69–92 cycles (the particular cycle depending on the sample).

Fig. 27 [78] shows the fractional change in contact electrical resistance during cyclic shear loading at a shear stress amplitude of 0.81 MPa (lower than that of Fig. 25). The resistance abruptly increases after 557–690 cycles (depending on the sample), due to bond degradation, which is not visually observable. Bond failure does not occur up to 1300 cycles, at which testing is stopped.

Comparison of Figs. 24, 26 and 27 shows that a higher stress amplitude causes bond degradation and bond failure to occur at lower number of cycles, as expected. The abrupt increase in resistance due to bond degradation (not bond failure) (Figs. 24, 26 and 27) provides a method of monitoring bond quality nondestructively in real time during dynamic loading. In contrast, bond strength measurement by mechanical testing is destructive. The bond degradation is attributed to fatigue. This interpretation is consistent with the absence of an abrupt resistance increase during static loading prior to failure.

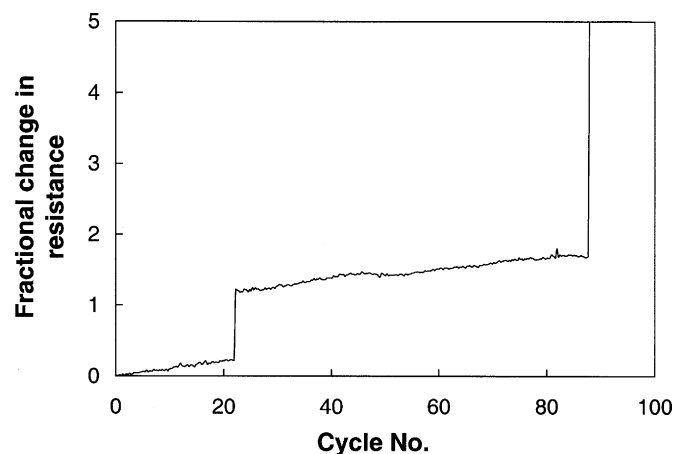


Fig. 26. Variation of the fractional contact resistance change with cycle number during cyclic shear loading of a joint between old and new mortars at a shear stress amplitude of 0.97 MPa up to bond failure. The contact resistance is that of the interface between old and new mortars.

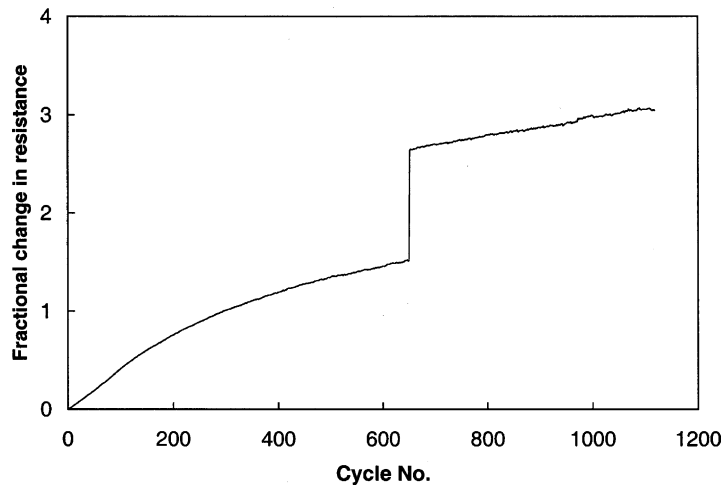


Fig. 27. Variation of the fractional contact resistance change with cycle number during cyclic shear loading of a joint between old and new mortars at a shear stress amplitude of 0.81 MPa. The test was stopped prior to bond failure. The contact resistance is that of the interface between old and new mortars.

### 2.5. Damage at the interface between unbonded concrete elements

Many concrete structures involve the direct contact of one cured concrete element with another, such that one element exerts static pressure on the other due to gravity. In addition, dynamic pressure may be exerted by live loads on the structure. An example of such a structure is a bridge involving slabs supported by columns, with dynamic live loads exerted by vehicles traveling on the bridge. Another example is a concrete floor in the form of slabs supported by columns, with live loads exerted by people walking on the floor. The interface between concrete elements that are in pressure contact is of interest, as it affects the integrity and reliability of the assembly. For example, deformation at the interface affects the interfacial structure, which can affect the effectiveness of load transfer between the contacting elements and can affect the durability of the interface to the environment. Moreover, deformation at the interface can affect the dimensional stability of the assembly. Of particular concern is how the interface is affected by dynamic loads.

Effective study of the interface between concrete elements that are in pressure contact and under dynamic loading requires the monitoring of the interface during dynamic loading. Hence, a nondestructive monitoring technique that provides information in real time during dynamic loading is desirable. Microscopic examination of the interface viewed at the edge cannot effectively provide interfacial information, though it can be nondestructive and be in real time. Microscopic examination of the interface surfaces after separation of the contacting elements can provide microstructural information, but it cannot be performed in real time. Mechanical testing of the interface, say under shear, can provide interfacial information, but it is destructive (unless the shear strain amplitude is within the elastic regime) and it cannot be conveniently performed in real time (due to the difficulty of having simultaneous dynamic compression and dynamic shear). The difficulties and ineffectiveness associated with these conventional techniques contribute to causing the scarcity of work on concrete–concrete pressure contacts.

In this section, contact electrical resistance measurement is used to monitor concrete–concrete pressure contacts in real time during dynamic pressure application. As the surface of concrete is never perfectly smooth, asperities occur on the surface, thus causing the true contact area at the interface to be much smaller than the geometric junction area. As a consequence, the local stress at

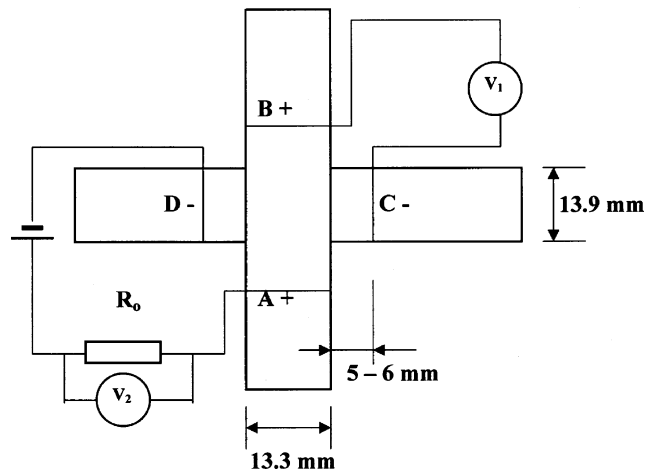


Fig. 28. Sample configuration for measurement of the contact electrical resistance of the interface between unbonded mortar elements.

the asperites is much higher than the overall stress applied to the junction. The greater the true contact area, the lower is the contact resistance. Deformation (flattening) of the asperites, as caused by the high local stress at the asperites, increases the true contact area. Therefore, the interfacial structure is changed. The contact resistance provides information on the interfacial structure, particularly in relation to the deformation at the interface. By monitoring the contact resistance in real time during loading and unloading, the extent, reversibility and loading history dependence of the deformation at various points of loading and unloading can be investigated, thus providing information on the structure and dynamic behavior of the interface.

Since concrete is somewhat conductive electrically, the contact resistance of the interface between contacting concrete elements can be conveniently measured by using the concrete elements as electrical leads—two for passing current and two for voltage measurement (i.e. the four-probe method), as provided by two concrete beams that overlap at  $90^\circ$  (Fig. 28). The volume resistance of each lead is negligible compared to the contact resistance of the junction, so the measured resistance (i.e. voltage divided by current) is the contact resistance. The contact resistance multiplied by the junction area gives the contact resistivity, which is independent of the junction area and describes the structure of the interface.

The data further [79] involves the use of mortar (with fine aggregate but not coarse aggregate) instead of concrete (with both fine and coarse aggregates). However, the interfacial effects should be quite similar for mortar and concrete.

Fig. 29 shows the variation in resistance and stress during cyclic compressive loading at a stress amplitude of 5.0 MPa. The compressive strength of the mortar used is  $64 \pm 2$  MPa, as determined by compressive testing of  $51 \text{ mm} \times 51 \text{ mm} \times 51 \text{ mm}$  (2 in.  $\times$  2 in.  $\times$  2 in.) cubes. The stress–strain curve is a straight line up to failure. In every cycle, the resistance decreases as the compressive stress increases, such that the maximum stress corresponds to the minimum resistance and the minimum stress (zero stress) corresponds to the maximum resistance. The minimum resistance (at the maximum stress) increases slightly as cycling progresses, but the maximum resistance (at the minimum or zero stress) decreases with cycling. Due to the asperites at the interface, the local compressive stress on the asperites is much higher than the overall compressive stress. As a result, plastic deformation occurs at the asperites, which means that more contact area is created during cycling. The occurrence of deformation is supported by the cross-head displacement observed within

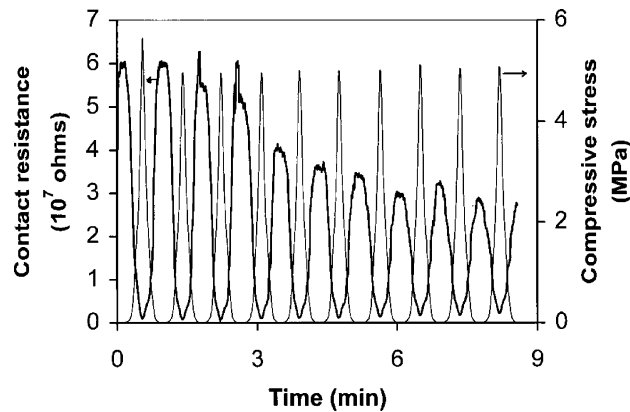


Fig. 29. Variation of contact resistance (thick curve) with time and of compressive stress (thin curve) with time during cyclic compression at a stress amplitude of 5 MPa. The contact resistance is that of the interface between unbonded mortar elements.

each cycle. The displacement is greatest (i.e. most deformation) at the maximum stress within each cycle and is not totally reversible. The plastic deformation is why the observed electrical resistance at the minimum stress (i.e. upon unloading) decreases as cycling progresses. On the other hand, due to the brittleness of the mortar, the compressive loading probably causes fracture at some of the asperites, thereby generating debris, which increases the contact resistance. Debris generation is probably the reason for the slight increase in the contact resistance at the maximum stress as cycling progresses. After about seven loading cycles, the maximum resistance (at the minimum stress) levels off, due to the limit of the extent of flattening of the asperites. However, the slight increase of the minimum resistance (at the maximum stress) persists beyond the first seven cycles, probably due to the continued generation of debris as cycling progresses.

The stress amplitude in Fig. 30 is 15 MPa, which is higher than that in Fig. 29. The minimum resistance (at the maximum stress) increases with cycling more significantly than in Fig. 29. This is probably due to the more significant debris generation at the higher stress amplitude. The maximum resistance (at the minimum stress) increases in the first four cycles. This is probably due to the effect of debris generation overshadowing the effect of the flattening of the asperites. After four cycles, the maximum resistance essentially levels off, probably due to the limit of the extent of debris generation for this stress amplitude.

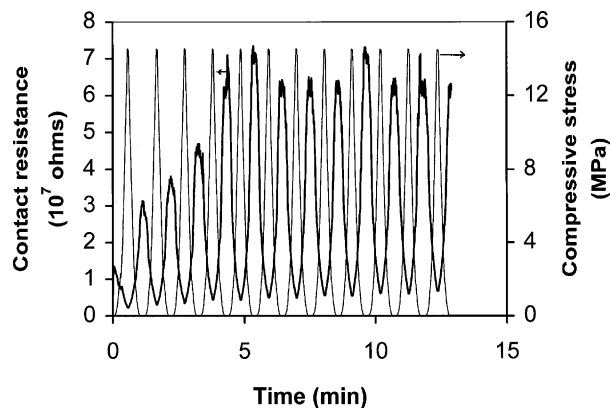


Fig. 30. Variation of contact resistance with time and of compressive stress with time during cyclic compression at a stress amplitude of 15 MPa. The contact resistance is that of the interface between unbonded mortar elements.

The results given earlier mean that, even at a low compressive stress amplitude of 5 MPa, the structure of a concrete–concrete contact changes during dynamic compression. Thus, the interfacial structure is dependent on the loading history. The debris generation at the interface may be of practical concern, as the load transfer between the contacting concrete elements may be affected by the debris.

#### *2.6. Damage at the interface between concrete and its carbon fiber–epoxy matrix composite retrofit*

Continuous fiber–polymer matrix composites are increasingly used to retrofit concrete structure, particularly columns [80–92]. The retrofit involves wrapping a fiber sheet around a concrete column or placing a sheet on the surface of a concrete structure, such that the fiber sheet is adhered to the underlying concrete using a polymer, most commonly epoxy. This method is effective for the repair of even quite badly damaged concrete structures. Although the fibers and polymer are very expensive compared to concrete, the alternative of tearing down and rebuilding the concrete structure is often even more expensive than the composite retrofit. Both glass fibers and carbon fibers are used for the composite retrofit. Glass fibers are advantageous for their relatively low cost, but carbon fibers are advantageous for their high tensile modulus.

The effectiveness of a composite retrofit depends on the quality of the bond between the composite and the underlying concrete, as good bonding is necessary for load transfer. Peel testing for bond quality evaluation is destructive [93]. Nondestructive methods to evaluate the bond quality are valuable. They include acoustic methods, which are not sensitive to small amounts of debonding or bond degradation [94], and dynamic mechanical testing [95]. This section uses electrical resistance measurement for nondestructive evaluation of the interface between concrete and its carbon fiber composite retrofit [96]. The method is effective for studying the effect of debonding stress on the interface. The concept behind the method is that bond degradation causes the electrical contact between the carbon fiber composite retrofit and the underlying concrete to degrade. Since concrete is electrically more conductive than air, the presence of an air pocket at the interface causes the measured apparent volume resistance of the composite retrofit in a direction in the plane of the interface to increase. Hence, bond degradation is accompanied by an increase in the apparent resistance of the composite retrofit. Although the polymer matrix (epoxy) is electrically insulating, the presence of a thin layer of epoxy at the interface was found to be unable to electrically isolate the composite retrofit from the underlying concrete.

A 40 mm × 15 mm sample of carbon fiber sheet (the composite retrofit), with the fibers along the 40 mm length of the sample, is pressed against a surface of the polished concrete block while the epoxy resin is at the interface for the purpose of bonding the fiber sheet to the concrete, as illustrated in Fig. 31 [96]. The curing of the epoxy resin is carried out at room temperature.

Four electrical contacts (A–D) are applied at four points along the 40 mm length of the fiber sheet sample, such that each contact is a strip stretching across the 15 mm width of the sample (Fig. 31). Each electrical contact is in the form of silver paint in conjunction with copper wire. In the four-probe method used for dc electrical resistance measurement, two of the electrical contacts (A and D, Fig. 31) are for passing current, and the remaining two contacts (B and C) are for measuring voltage. The voltage divided by the current gives the measured resistance, which is the apparent volume resistance of the fiber sheet between B and C when the sheet is in contact with the concrete substrate.

Uniaxial compression is applied on a concrete block with fiber sheet on one surface, such that the stress is in the fiber direction (Fig. 31), while the electrical resistance is continuously measured.

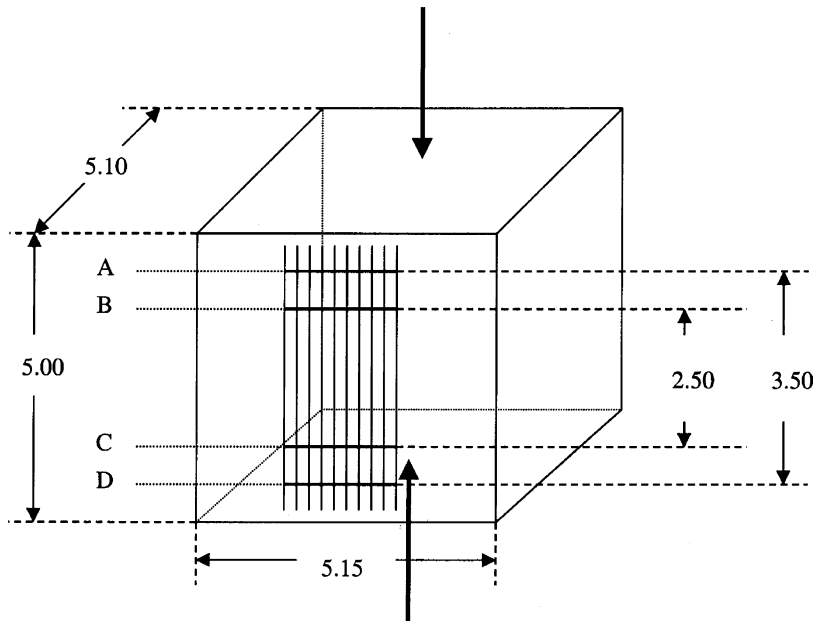


Fig. 31. Sample configuration. The vertical arrow indicates the direction of compressive loading. All dimensions are in cm. A–D are the four electrical leads emanating from the four electrical contacts (thick horizontal lines), which are attached to the fiber retrofit indicated by vertical parallel lines on the front face of the concrete block. The fiber direction is in the stress direction (vertical).

Fig. 32 shows the fractional change in resistance during cyclic compressive loading at a stress amplitude of 1.3 MPa. The stress is along the fiber direction. Stress returns to zero at the end of each cycle. In each cycle, the electrical resistance increases reversibly during compressive loading. This is attributed to the reversible degradation of the bond between carbon fiber sheet and concrete substrate during compressive loading. This bond degradation decreases the chance for fibers to touch the concrete substrate, thereby leading to a resistance increase.

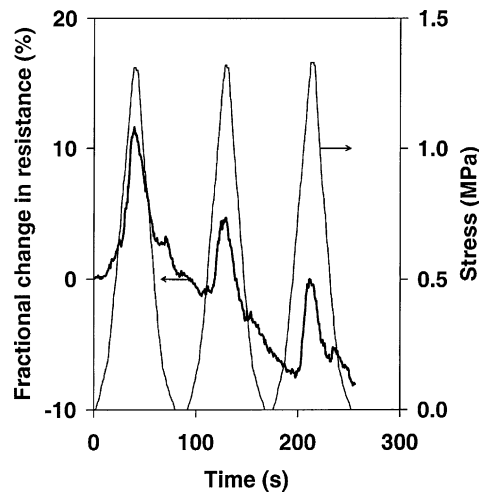


Fig. 32. The fractional change in resistance for the fiber retrofit on a concrete substrate during cyclic compressive loading.

As cycling progresses, both the maximum and minimum values of the fractional change in resistance in a cycle decreases. This is attributed to the irreversible disturbance in the fiber arrangement during repeated loading and unloading. This disturbance increases the chance for fibers to touch the concrete substrate, thereby causing the resistance to decrease irreversibly as cycling progresses.

As shown in Fig. 32, the first cycle exhibits the highest value of the fractional change in resistance. This is due to the greatest extent of bond degradation taking place during the first cycle.

### 3. Damage due to freeze–thaw cycling in a cement-based material

Freeze–thaw cycling is one of the main causes of degradation of concrete in cold regions. The degradation stems from the freezing of the water in the concrete upon cooling, and the thawing upon subsequent heating. The phase transition is accompanied by dimensional change and internal stress change. Freeze–thaw cycling can result in failure.

Research on the freeze–thaw durability of cement-based materials has been focused on the mechanical property degradation (e.g. modulus and strength) [97–99], weight change [97,99–101], length change [101,102], microstructural change [103] and ultrasonic signature change [101,104] after different amounts of freeze–thaw cycling. Relatively little attention has been previously given to monitoring during freeze–thaw cycling. Techniques previously used for real-time monitoring include strain measurement [102] and electrical resistivity measurement [105]. Without real-time monitoring, the degradation could not be monitored during freeze–thaw cycling. Therefore, study of the damage evolution required testing numerous specimens at different number of freeze–thaw cycles. As different specimens are bound to be a little different in the degree of perfection, the testing of different specimens gives data scatter which makes it difficult to study the damage evolution. In order to study the damage evolution on a single specimen during freeze–thaw cycling, a nondestructive and sensitive real-time testing method is necessary.

Electrical resistivity measurement is a nondestructive method. The electrical resistivity of cement paste decreases reversibly upon heating at temperature above 0 °C (without freezing or thawing), due to the existence of an activation energy for electrical conduction [106]. This phenomenon allows cement paste to function as a thermistor for sensing temperature. Thus, electrical resistivity measurement allows simultaneous monitoring of both temperature and damage. A temperature increase causes the resistivity to decrease reversibly, whereas damage causes the resistivity to increase irreversibly.

Fig. 33 [107] shows the fractional change in resistivity and the temperature during fast thermal cycling (40 min per cycle) of mortar (without fiber) between –20 and 52 °C. The resistivity decreases upon heating and increases upon cooling in every cycle, due to the existence of an activation energy for electrical conduction. The resistivity changes smoothly and similarly above and below 0 °C, indicating that the phase transition does not affect the resistivity. Even when the heating and cooling rates are very low, i.e. 6 h per cycle, the phase transition at 0 °C has only slight effect on the resistivity (Fig. 34). Although the resistivity changes abruptly at 0 °C, the effects of freezing and thawing on the resistivity are small compared to the effect of temperature on the resistivity. It is reasonable that this small effect is only observed when the heating and cooling rates are low.

The resistivity at the end of a heating–cooling cycle is higher than that at the beginning of the cycle (Fig. 33). In other words, the upper envelope of the resistivity variation (corresponding to the resistivity at –20 °C) increases cycle by cycle. The lower envelope (corresponding to the resistivity at 52 °C) also increases cycle by cycle, but the increase is less significant than that of the upper

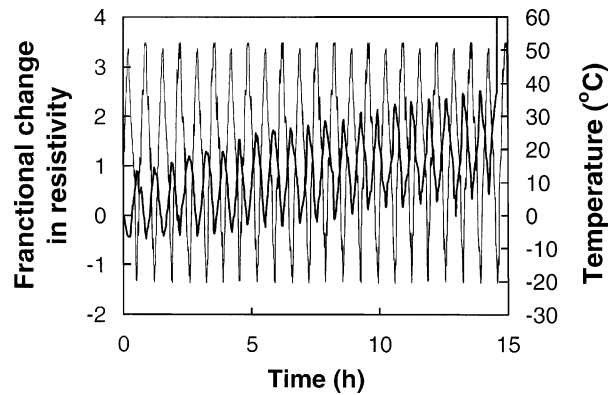


Fig. 33. The fractional change in resistivity vs. time (thick curve) and the temperature vs. time (thin curve) during fast freeze–thaw cycling (40 min per cycle) of mortar (without fiber).

envelope. As a consequence, the amplitude of resistivity variation increases with cycling. This behavior is attributed to damage, which causes the resistivity to increase irreversibly. That the upper envelope upshifts more than the lower envelope means that the damage occurs more significantly upon cooling than upon heating. This is expected since: (i) thermal contraction occurs upon cooling and the surface of the specimen cools faster than the center of the specimen; and (ii) water expands upon freezing.

Upon freeze–thaw failure, the resistivity rises abruptly to essentially infinity, as observed before the completion of 15 h of cycling (Fig. 33). This rise occurs at  $-20^{\circ}\text{C}$  (the coldest point of a cycle), again indicating that damage during cooling is more significant than that during heating. Prior to failure, no abrupt resistivity increase was observed. This means that the damage evolution involves damage accumulating gradually cycle by cycle, until failure occurs.

At a given temperature, the resistivity during heating is slightly lower than that during subsequent cooling, as shown in Fig. 34. The hysteresis becomes more severe as cycling progresses. The hysteresis is attributed to the damage inflicted during cooling and the association of damage with a higher resistivity. That damage infliction occurs smoothly throughout cooling from  $52$  to  $-20^{\circ}\text{C}$  means that the damage is not due to freezing itself, but is due to thermal contraction and the fact that the surface cools faster than the center of the specimen.

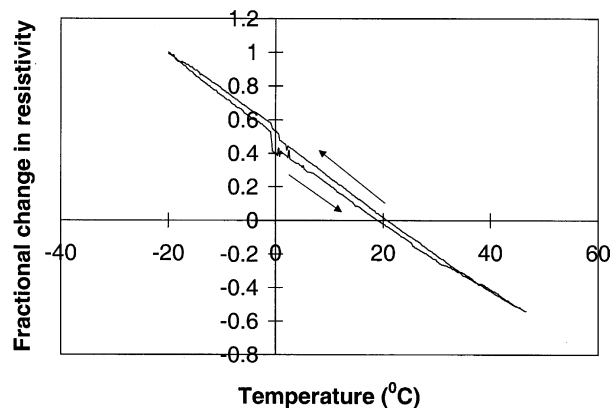


Fig. 34. The fractional change in resistivity vs. temperature in a cycle of slow freeze–thaw cycling (6 h per cycle) of mortar (without fiber).

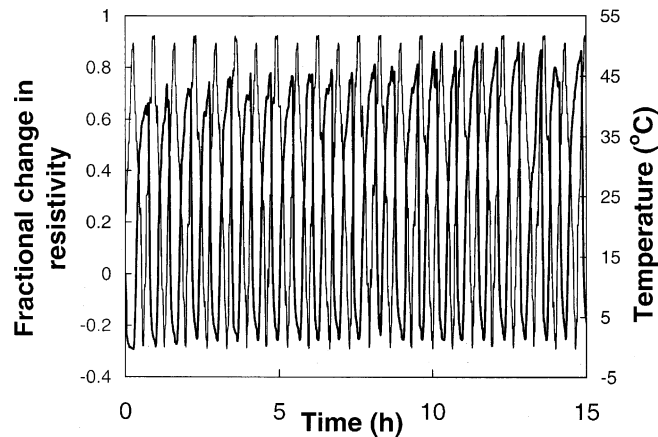


Fig. 35. The fractional change in resistivity vs. time (thick curve) and the temperature vs. time (thin curve) during temperature cycling of mortar (without fiber) without freezing.

Fig. 35 shows the fractional change in resistivity and the temperature during fast thermal cycling (40 min per cycle) between 0 and 52 °C (i.e. without freezing). The resistivity decreases reversibly upon heating, due to the existence of an activation energy for electrical conduction. In contrast to the case of freeze–thaw cycling at a similar cycling rate (Fig. 33), the lower envelope of resistivity variation does not shift upon cycling and the upper envelope upshifts only slightly. As the irreversible increase in resistivity is associated with damage, this means that the damage during thermal cycling without freezing is negligible compared to that during freeze–thaw cycling. As a result, failure does not occur after 15 h of thermal cycling without freezing, but was visually observed before the end of 15 h of freeze–thaw cycling (Fig. 33).

As mentioned earlier, the damage in Fig. 33 was not due to freezing itself, but was due to thermal contraction and the fact that the surface cooled faster than the center of the specimen. Comparison between Figs. 33 and 35 shows that the damage caused by thermal contraction is significant in the presence of freezing, but negligible in the absence of freezing. In other words, freezing aggravates the damage that is due to thermal contraction.

The thermal damage observed in Fig. 33 is not related to damage that occurs at elevated temperatures (up to 52 °C). This is shown by a separate experiment in which the resistivity was monitored over time up to 4000 s at a constant temperature of 50 °C. The resistivity was observed to increase by less than 2%, in contrast to the much larger fractional increase in resistivity (whether the upper envelope or the lower envelope) in Fig. 33.

#### 4. Damage due to creep in a cement-based material

Creep [108,109] is a form of time-dependent plastic deformation that occurs under load, which is typically fixed during creep testing. Creep affects the dimensions of a component and dimensional stability is important for many structural components, including concrete slabs and columns. Although creep during concrete curing [110–115] is more significant than that after curing [116–120], creep after curing is relevant to the durability and stability of structures during use. Thus, this section addresses creep after curing. Creep is more severe at elevated temperatures [121,122], but this section is limited to creep at room temperature.

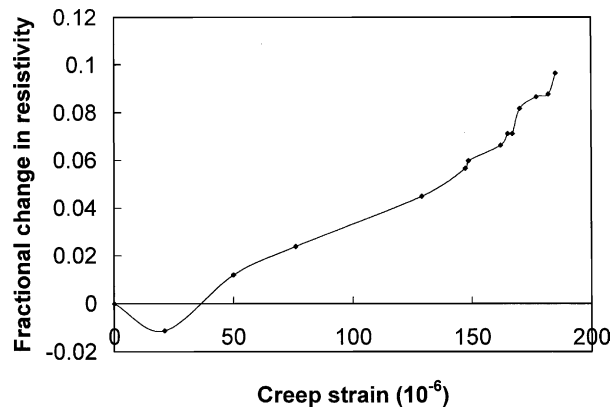


Fig. 36. Fractional change in resistivity vs. compressive strain during a month of creep testing of plain cement mortar at a constant compressive stress.

Research on creep has been focused on the strain during creep [123–127], rather than the material property variation during creep. The microstructure affects numerous properties, including mechanical and electrical properties. For the purpose of understanding the microstructural effect of creep, it is desirable to investigate the property variation during creep. It is further preferred that the property be measurable nondestructively, so that the same specimen can be monitored throughout the creep process. This section uses the electrical resistivity as the property for nondestructive measurement. Prior work that involved monitoring a material property during creep was limited to the stiffness [128] and the ultrasonic pulse velocity [129].

The creep resistance of cement-based materials is affected by admixtures such as silica fume [130–133], fly ash [130,132,134], slag [132] and steel fibers [135,136]. However, this section does not address the effect of admixtures.

Fig. 36 [137] shows the fractional change in electrical resistivity in the stress direction during creep testing at a constant compressive stress (20 MPa, compared to the compressive strength of 51 MPa) for plain cement mortar in the cured state (28 days of curing). The fractional change in resistivity is essentially equal to the fractional change in resistance due to the small strain involved.

The resistivity increases as creep progresses except for the initial stage of creep, in which the resistivity drops slightly. The initial drop in resistivity is slight and does not occur in all the specimens. It is believed to be due to stress-induced healing of defects (Section 2.1.1).

The main effect of creep is the increase on resistivity, which is attributed to microstructural change, which can be viewed as minor damage. The fractional change in resistivity per unit strain is 500. This value is about the same for specimens which do not exhibit the initial drop in resistivity. The fractional change in resistivity per unit strain reflects the extent of creep-induced microstructural change. The value of 500 is comparable to that for drying shrinkage (Section 5) and is larger than the value of 250 (or less) for static compressive strain (i.e. instantaneous strain rather than creep strain) (Fig. 15) [45]. This means that the extent of creep-induced microstructural change is comparable to that of drying shrinkage-induced microstructural change and is larger than that of stress-induced microstructural change.

The effect of creep on the resistivity is consistent with the effect of strain rate on the resistivity (Section 2.1.4); the lower the strain rate, the higher is the fractional change in resistivity at the same strain (Fig. 15).

## 5. Damage due to drying shrinkage in a cement-based material

The hydration reaction that occurs during the curing of cement causes shrinkage, called autogenous shrinkage. In case that the curing is conducted in an open atmosphere, as is usually the case, additional shrinkage occurs due to the movement of water through the pores to the surface and the loss of water on the surface by evaporation. This is drying shrinkage.

The drying shrinkage of cement-based materials is a cause of defects (such as cracks) in cement-based materials. It can also cause pre-stressing loss [138]. The tendency for defect formation during shrinkage increases with increasing size of the cement-based material. Thus, the problem is particularly serious for large concrete structures such as floors and dams.

The effects of drying shrinkage have been studied by numerous workers by measurement of the shrinkage strain and observation of the cracks. However, the microstructural change, which necessarily proceeds the cracking, has not received much attention. The extent of microstructural change and the evolution of the microstructure as shrinkage occurs are important for the understanding of the shrinkage process. This understanding is valuable for the alleviation of the problem associated with shrinkage-induced cracking.

Silica fume [139–142] is very fine non-crystalline silica produced by electric arc furnaces as a byproduct of the production of metallic silicon or ferrosilicon alloys. It is a powder with particles having diameter 100 times smaller than those of anhydrous Portland cement particles, i.e. mean particle size between 0.1 and 0.2  $\mu\text{m}$ . The  $\text{SiO}_2$  content ranges from 85 to 98%. Silica fume is pozzolanic.

Silica fume used as an admixture in a concrete mix has significant effects on the properties of the resulting material [143]. These effects pertain to the strength, modulus, ductility, vibration damping capacity, sound absorption, abrasion resistance, air void content, shrinkage, bonding strength with reinforcing steel, permeability, chemical attack resistance, alkali–silica reactivity reduction, corrosion resistance of embedded steel reinforcement, freeze–thaw durability, creep rate, coefficient of thermal expansion, specific heat, thermal conductivity, defect dynamics, dielectric constant, and degree of fiber dispersion in mixes containing short microfibers. In addition, silica fume addition degrades the workability of the mix.

The addition of untreated silica fume to cement paste decreases the drying shrinkage [138,144–149]. This desirable effect is partly due to the reduction of the pore size and connectivity of the voids and partly due to the pre-stressing effect of silica fume, which restrains the shrinkage. The use of silane-treated silica fume in place of untreated silica fume further decreases the drying shrinkage, due to the hydrophilic character of the silane-treated silica fume and the formation of chemical bonds between silica fume particles and cement [138]. The use of silane and untreated silica fume as two admixtures also decreases the drying shrinkage, but not as significantly as the use of silane-treated silica fume [138]. However, silica fume has also been reported to increase the drying shrinkage [139,150,151] and the restrained shrinkage crack width is increased by silica fume addition [152].

Due to the pozzolanic nature of silica fume, silica fume addition increases the autogenous shrinkage, as well as the autogenous relative humidity change [153,154]. These effects are undesirable, as they may cause cracking if the deformation is restrained. Aggregates are known to decrease the drying shrinkage [155].

In order to study the effects of silica fume and fine aggregate on the shrinkage-induced microstructural change, this section addresses the drying shrinkage of cement pastes with and without silica fume (untreated) and of mortar without silica fume. Both the shrinkage strain and the electrical resistivity (related to the microstructure and obtained from the electrical resistance and the strain) were measured continually from 1 to 28 days of curing [156].

Table 2  
Volume electrical resistivity and resistance at 1 day of curing

Material	Resistivity ( $\Omega$ cm)	Resistance (M $\Omega$ )	Water/cement ratio
Plain cement paste	$1.01 \times 10^6$	0.233	0.30
Plain cement paste	$1.06 \times 10^6$	0.244	0.35
Plain cement paste	$1.11 \times 10^6$	0.257	0.40
Cement paste with silica fume	$5.46 \times 10^5$	0.126	0.35
Mortar (with sand)	$1.56 \times 10^7$	3.59	0.35

Table 2 shows the initial (1 day of curing) values of the volume electrical resistivity and resistance for each of the five compositions investigated [156]. The resistivity increases with increasing water/cement ratio. It is decreased by the addition of silica fume and is increased by the addition of sand.

Figs. 37 and 38 show the shrinkage strain and fractional change, respectively, in resistivity versus curing age. The presence of silica fume decreases both shrinkage strain and fractional change in resistivity at the same curing age for all curing ages from 1 to 28 days. This means that the silica fume restrains the drying shrinkage as well as the shrinkage-induced microstructural change. Both shrinkage strain and fractional change in resistivity increase smoothly with increasing curing age, such that the increase becomes more gradual as curing progresses.

Sand decreases the shrinkage strain even more than silica fume (Fig. 37), but the fractional change in resistivity is increased by sand. This means that the shrinkage-induced microstructural change is larger when sand is present, presumably due to the effect of shrinkage on the microstructure of the interface between sand and cement. Sand does not shrink while cement shrinks, thereby resulting in microstructural change at the sand–cement interface as drying shrinkage proceeds. The interface is associated with a contact electrical resistance, which increases as the interfacial voids or void precursors become more numerous. The increase of the contact resistivity between steel rebar and concrete as drying shrinkage proceeds has been reported [68].

An increase in the water/cement ratio causes a negligible increase in the shrinkage strain (Fig. 37), but a slight increase in the fractional change in resistivity (Fig. 38), as shown by comparing the three plain cement pastes with water/cement ratios of 0.30, 0.35 and 0.40. This means that the

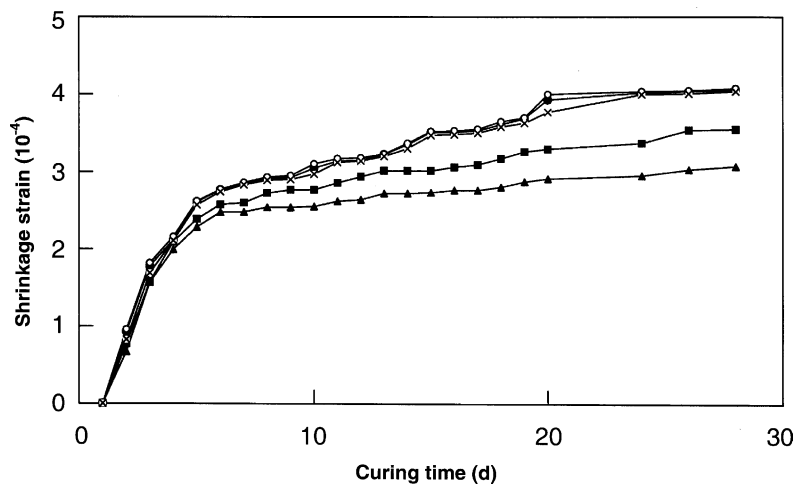


Fig. 37. Shrinkage strain vs. curing time for plain cement paste with water/cement ratio = 0.30 (x), plain cement paste with water/cement ratio = 0.35 (●), plain cement paste with water/cement ratio = 0.40 (○), silica fume cement paste (■), and plain mortar (▲).

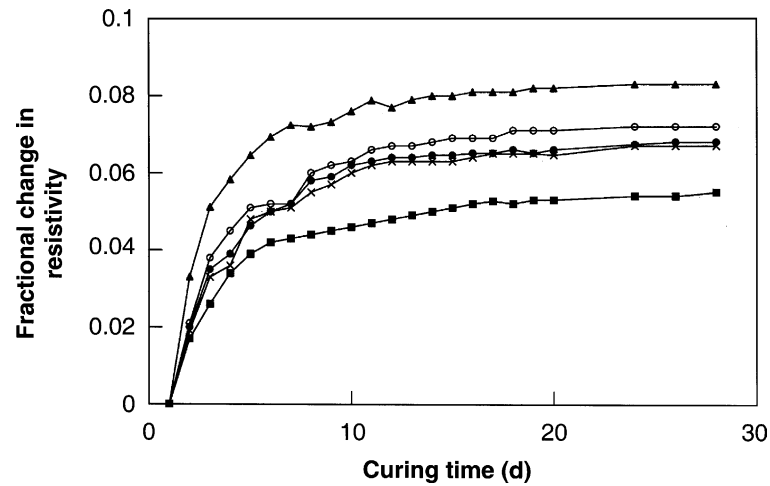


Fig. 38. Fractional change in resistivity vs. curing time for plain cement paste with water/cement ratio = 0.30 (×), plain cement paste with water/cement ratio = 0.35 (●), plain cement paste with water/cement ratio = 0.40 (○), silica fume cement paste (■), and plain mortar (▲).

shrinkage-induced microstructural change increases slightly with increasing water/cement ratio. The effect of the water/cement ratio is much smaller than that of silica fume or sand.

Fig. 39 shows that the fractional change in resistivity is less in the presence of silica fume for the same strain. This implies that the extent of microstructural change at the same strain is less in the presence of silica fume. Fig. 39 also shows that the fractional change in resistivity is higher in the presence of sand for the same strain. Thus, the extent of microstructural change at the same strain is more in the presence of sand.

Fig. 39 shows that the fractional change in resistivity abruptly increases at a strain of  $3.0 \times 10^{-4}$  for all cement pastes without silica fume and at a strain of  $2.5 \times 10^{-4}$  for mortar. This abrupt resistivity increase is probably associated with an abrupt and irreversible microstructural change. The addition of silica fume essentially eliminates this effect, whereas the addition of sand causes the

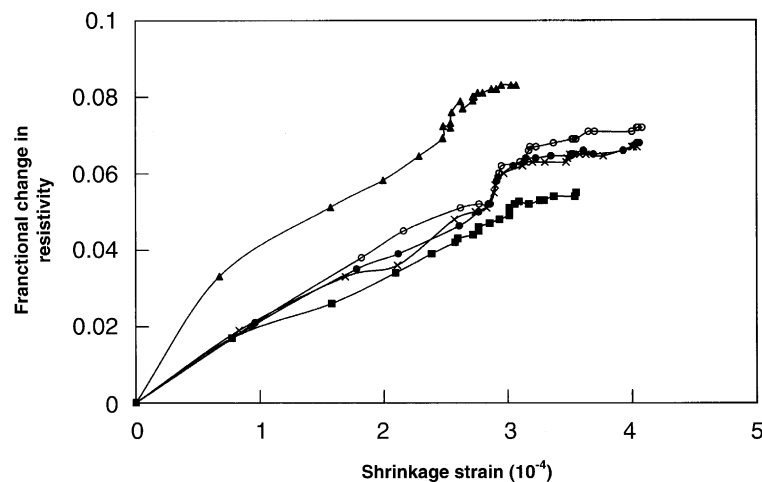


Fig. 39. Fractional change in resistivity vs. shrinkage strain for plain cement paste with water/cement ratio = 0.30 (×), plain cement paste with water/cement ratio = 0.35 (●), plain cement paste with water/cement ratio = 0.40 (○), silica fume cement paste (■), and plain mortar (▲).

microstructural change to occur at a lower shrinkage strain. This is consistent with the notion that silica fume addition diminishes the shrinkage-induced microstructural change, whereas sand addition increases this quantity.

The fractional change in resistivity per unit strain is in the range from 150 to 500. This quantity describes the severity of shrinkage-induced microstructural change. The severity is slightly lower in the presence of silica fume, and is significantly higher in the presence of sand. The severity tends to decrease as shrinkage proceeds, as expected from the decreasing rate of shrinkage as shrinkage proceeds (Fig. 37).

The fractional change in resistivity per unit compressive strain in the cured state, as determined during compressive loading, is 10 [30]. Thus, the microstructural change induced by shrinkage strain is much larger than that induced by compressive strain for the same amount of strain. Nevertheless, both shrinkage strain and compressive strain cause the resistivity in the strain direction to increase. The large microstructural change during drying shrinkage is expected from the hydration reaction which takes place during curing.

## 6. Conclusion

Electrical resistivity measurement provides a means of sensing the damage (or microstructural changes) in a cement-based material in real time. Damage is shown by an increase in the resistivity. For indicating the damage within the cement-based material, the volume resistivity is the relevant quantity. For indicating damage at the interface between steel rebar and concrete, between old concrete and new concrete, and between unbonded concrete elements, the contact resistivity is the relevant quantity. For indicating the damage at the interface between concrete and its carbon fiber–epoxy matrix composite retrofit, the apparent volume resistivity of the retrofit is the relevant quantity.

The fractional change in volume resistivity per unit strain is a parameter that describes the extent of strain-induced microstructural change in a cement-based material. This extent is thus found to be much larger for compressive creep and drying shrinkage than static compressive deformation. Creep occurs over time, thus allowing relatively extensive microstructural change to take place. Drying shrinkage is accompanied by the hydration reaction, which is necessarily accompanied by extensive microstructural change.

During static compression of mortar, the extent of microstructural change at a given strain, as indicated by the fractional change in resistivity, decreases with increasing loading rate. This is because it takes time for microstructural change to occur. The need for time is also indicated by the large effect observed during creep.

Freeze–thaw cycling causes damage, which progresses cycle by cycle and occurs in each cycle more significantly upon cooling than upon heating, as shown by the resistivity at the coldest point of a cycle increasing upon cycling more than that at the warmest point of a cycle.

In contrast to damage, which causes the volume resistivity to increase, defect healing causes this resistivity to decrease. Defect healing occurs during compression, but subsequent unloading annuls the healing and aggravates the damage.

## References

- [1] V. Pensee, D. Kondo, L. Dormieux, *J. Eng. Mech.* 128 (8) (2002) 889–897.
- [2] F. Ragueneau, Ch. La Borderie, J. Mazars, *Mech. Cohesive-Frictional Mater.* 5 (8) (2000) 607–625.
- [3] R. Mahnken, D. Tikhomirov, E. Stein, *Comput. Struct.* 75 (2) (2000) 135–143.

- [4] L. Gao, C.-T.T. Hsu, *ACI Mater. J.* 95 (5) (1998) 575–581.
- [5] A. Litewka, J. Bogucka, J. Debinski, *Arch. Civil Eng.* 42 (4) (1997) 425–445.
- [6] S. Murakami, K. Kamiya, *Int. J. Mech. Sci.* 39 (4) (1997) 473–486.
- [7] E. Papa, A. Taliercio, *Eng. Fract. Mech.* 55 (2) (1996) 163–179.
- [8] D.J. Stevens, D. Liu, *J. Eng. Mech. ASCE* 118 (6) (1992) 1184–1200.
- [9] D. Breyse, N. Schmitt, *Cem. Concr. Res.* 21 (6) (1991) 963–974.
- [10] S. Yazdani, H.L. Schreyer, *J. Eng. Mech. ASCE* 116 (7) (1990) 1435–1450.
- [11] W. Suaris, C. Ouyang, V.M. Fernando, *J. Eng. Mech. ASCE* 116 (5) (1990) 1020–1035.
- [12] D. Breyse, *Struct. Saf.* 8 (1–4) (1990) 311–325.
- [13] H. Watanabe, Y. Murakami, M. Ohtsu, *Zairyo (J. Soc. Mater. Sci. Jpn.)* 50 (12) (2001) 1370–1374.
- [14] H. Ji, T. Zhang, M. Cai, Z. Zhang, *Yanshilixue Yu Gongcheng Xuebao (Chin. J. Rock Mech. Eng.)* 19 (2) (2000) 165–168.
- [15] E.N. Landis, *Construction Building Mater.* 13 (1) (1999) 65–72.
- [16] T.J. Mackin, M.C. Roberts, *J. Am. Ceram. Soc.* 83 (2) (2000) 337–343.
- [17] Y. Chen, N. Li, A. Li, Y. Pu, Q. Liao, *Yanshilixue Yu Gongcheng Xuebao (Chin. J. Rock Mech. Eng.)* 19 (6) (2000) 702–706.
- [18] H.I. Schreyer, M.K. Neilsen, in: *Proceedings of the ASCE Engineering and Mechanics Specialty Conference on Mechanics Computing in 1990s and Beyond*, ASCE, New York, NY, 1991, pp. 303–307.
- [19] H. Cordes, D. Bick, *Beton und Stahlbetonbau* 86 (8) (1991) 181.
- [20] H. Meichsner, *Beton und Stahlbetonbau* 87 (4) (1992) 95.
- [21] A. Mor, P.J.M. Monteiro, W.T. Hester, *Cem. Concr. Aggregates* 11 (2) (1989) 121.
- [22] C. Edvardsen, *Betonwerk und Fertigteile-Technik* 62 (11) (1996) 77.
- [23] S. Jacobsen, J. Marchand, L. Boisvert, *Cem. Concr. Res.* 26 (6) (1996) 869.
- [24] S. Jacobsen, E.J. Sellevold, *Cem. Concr. Res.* 26 (1) (1996) 55.
- [25] S. Jacobsen, J. Marchand, H. Hornain, *Cem. Concr. Res.* 25 (8) (1995) 1781.
- [26] N. Hearn, *Mater. Struct.* 31 (212) (1998) 563.
- [27] C.M. Dry, in: *Proceedings of the Third International Conference on Intelligent Materials and Third European Conference on Smart Structures and Materials*, vol. 958, The International Society for Optical Engineering, Society of Photo-Optical Instrumentation Engineers (SPIE), Bellingham, WA, 1996, p. 2779.
- [28] C.M. Dry, in: *Proceedings of the Third International Conference on Intelligent Materials and Third European Conference on Smart Structures and Materials*, vol. 247, The International Society for Optical Engineering, Society of Photo-Optical Instrumentation Engineers (SPIE), Bellingham, WA, 1996, p. 2719.
- [29] C. Dry, *Smart Mater. Struct.* 3 (2) (1994) 118.
- [30] J. Cao, S. Wen, D.D.L. Chung, *J. Mater. Sci.* 36 (18) (2001) 4351–4360.
- [31] Z. Bayasi, J. Zhou, *ACI Mater. J.* 90 (4) (1993) 349.
- [32] B. Ma, J. Li, J. Peng, J. Wuhan, *Univ. Technol. Mater. Sci. Ed.* 14 (2) (1999) 1.
- [33] K. Tan, X. Pu, *Cem. Concr. Res.* 28 (12) (1998) 1819.
- [34] L. Bagel, *Cem. Concr. Res.* 28 (7) (1998) 1011.
- [35] C.A. Ross, in: *Proceedings of the 1997 ASME Pressure Vessels and Piping Conference on Structures Under Extreme Loading Conditions*, vol. 351, Pressure Vessels and Piping Division, American Society of Mechanical Engineers, New York, NY, 1997, pp. 255–262.
- [36] R. John, S.P. Surendra, *Fracture of concrete and rock*, in: *Proceedings of the SEM-RILEM International Conference*, Society for Experimental Mechanics Inc., Bethel, CT, 1987, pp. 35–52.
- [37] S. Ohgishi, H. Ono, *Zairyo (J. Soc. Mater. Sci. Jpn.)* 29 (318) (1980) 279–285.
- [38] Z. Li, Y. Huang, *ACI Mater. J.* 95 (5) (1998) 512–518.
- [39] S. Mindess, *Application of Fracture Mechanics to Cementitious Composites*. Series E. Applied Sciences, vol. 94, NATO ASI Series, Martinus Nijhoff, Dordrecht, The Netherlands, 1994, pp. 617–636.
- [40] J.-I. Takeda, *Cement-based composites: strain rate effects on fracture*, in: *Proceedings of the Symposium of the Materials Research Society*, vol. 64, Materials Research Society, Pittsburgh, PA, 1985, pp. 15–20.
- [41] D. Chandra, in: *Proceedings of the 10th Conference on Engineering and Mechanics*, vol. 1, ASCE, New York, NY, 1995, pp. 102–105.
- [42] D. Chandra, T. Krauthammer, *Earthquake Eng. Struct. Dyn.* 24 (12) (1995) 1609–1622.
- [43] J.-H. Yon, N.M. Hawkins, A.S. Kobayashi, *ACI Mater. J.* 89 (2) (1992) 146–153.
- [44] E. Pozzo, *Mater. Struct.* 20 (118) (1987) 303–314.
- [45] J. Cao, D.D.L. Chung, *Cem. Concr. Res.* 32 (5) (2002) 817–819.
- [46] P. Chen, D.D.L. Chung, *Composites B* 27 (1996) 11–23.
- [47] X. Fu, D.D.L. Chung, *Cem. Concr. Res.* 26 (1) (1996) 15–20.
- [48] D. Bontea, D.D.L. Chung, G.C. Lee, *Cem. Concr. Res.* 30 (4) (2000) 651–659.
- [49] F. Reza, G.B. Batson, J.A. Yamamuro, J.S. Lee, *Concrete: Materials Science to Applications. A Tribute to Surendra P. Shah*, ACI Publication SP 206, American Concrete Institute, Farmington Hills, MI, 2002, pp. 429–438.
- [50] Z. Li, M. Xu, N.C. Chung, *Mag. Concr. Res.* 50 (1) (1998) 49–57.

- [51] V.A. Ghio, P.J.M. Monteiro, *ACI Mater. J.* 94 (2) (1997) 111–118.
- [52] C.K. Kankam, *J. Struct. Eng. ASCE* 123 (1) (1997) 79–85.
- [53] H.P. Schroeder, T.B. Wood, *J. Cold Regions Eng.* 10 (2) (1996) 93–117.
- [54] N.M. Ihekweba, B.B. Hope, C.M. Hansson, *Cem. Concr. Res.* 26 (2) (1996) 267–282.
- [55] A.A. Almusallam, A.S. Al-Gahtani, A.R. Aziz, *Construction Building Mater.* 10 (2) (1996) 123–129.
- [56] B.S. Hamad, *ACI Mater. J.* 92 (6) (1995) 579–590.
- [57] A. Hamouine, M. Lorrain, *Mater. Struct.* 28 (184) (1995) 569–574.
- [58] K. Thangavel, N.S. Rengaswamy, K. Balakrishnan, *Indian Concr. J.* 69 (5) (1995) 289–293.
- [59] B.S. Hamad, *ACI Struct. J.* 92 (1) (1995) 3–13.
- [60] F. de Larrard, I. Schaller, J. Fuchs, *ACI Mater. J.* 90 (4) (1993) 333–339.
- [61] A.R. Cusens, Z. Yu, *Cem. Concr. Compos.* 14 (4) (1992) 269–276.
- [62] A.R. Cusens, Z. Yu, *Struct. Eng.* 71 (7) (1993) 117–124.
- [63] A. Mor, *ACI Mater. J.* 89 (1) (1992) 76–82.
- [64] M. Maslehuddin, I.M. Allam, G.J. Al-Sulaimani, A. Al-Mana, S.N. Abduljawwad, *ACI Mater. J.* 87 (5) (1990) 496–502.
- [65] C.-H. Chiang, C.-L. Tsai, Y.-C. Kan, *Ultrasonics* 38 (1) (2000) 534–536.
- [66] G.L. Balazs, C.U. Grosse, R. Koch, H.W. Reinhardt, *Mag. Concr. Res.* 48 (177) (1996) 311–320.
- [67] C.-H. Chiang, C.-K. Tang, *Ultrasonics* 37 (3) (1999) 223–229.
- [68] X. Fu, D.D.L. Chung, *ACI Mater. J.* 95 (6) (1998) 725–734.
- [69] J. Cao, D.D.L. Chung, *Cem. Concr. Res.* 31 (4) (2001) 669–671.
- [70] G.K. Ray, *Concr. Int.: Des. Construction* 9 (6) (1987) 24–28.
- [71] E.K. Schrader, *Concr. Int.: Des. Construction* 14 (11) (1992) 54–59.
- [72] C. Ozyildirim, in: V.M. Malhotra (Ed.), *ACI SP-132, American Concrete Institute, Detroit, 1992, 1287 pp.*
- [73] M.D. Luther, *Transp. Res. Rec.* 1204 (1988) 11–20.
- [74] D.G. Manning, J. Ryell, *Transp. Res. Rec.* 762 (1980) 1–9.
- [75] L. Calvo, M. Meyers, *Concr. Int.: Des. Construction* 13 (7) (1991) 46–47.
- [76] J.K. Bhargava, in: D.W. Fowler, L.E. Kukacka (Eds.), *ACI SP-69, American Concrete Institute, Detroit, 1981, 205 pp.*
- [77] P.-W. Chen, X. Fu, D.D.L. Chung, *Cem. Concr. Res.* 25 (3) (1995) 491–496.
- [78] J. Cao, D.D.L. Chung, *Cem. Concr. Res.* 31 (11) (2001) 1647–1651.
- [79] X. Luo, D.D.L. Chung, *Cem. Concr. Res.* 30 (2) (2000) 323–326.
- [80] H.A. Toutanji, *Compos. Struct.* 44 (2) (1999) 155–161.
- [81] H.A. Toutanji, T. El-Korchi, *J. Compos. Construction* 3 (1) (1999) 38–45.
- [82] Y. Lee, S. Matsui, *Tech. Rep. Osaka Univ.* 48 (2319–2337) (1998) 247–254.
- [83] E.K. Lau, A.S. Mosallam, P.R. Chakrabarti, in: *Proceedings of the International SAMPE Technical Conference, vol. 30, SAMPE, Covina, CA, 1998, pp. 293–302.*
- [84] A. Liman, P. Hamelin, in: *Proceedings of the International Conference on Computer Methods in Composite Materials (CADCOMP), Computational Mechanics Publishers, Ashurst, UK, 1998, pp. 569–578.*
- [85] P. Balaguru, S. Kurtz, in: *Proceedings of the International Seminar on Repair and Rehabilitation of Reinforced Concrete Structures: The State of the Art, ASCE, Reston, VA, 1998, pp. 155–168.*
- [86] A. Nanni, W. Gold, in: *Proceedings of the International Seminar on Repair and Rehabilitation of Reinforced Concrete Structures: The State of the Art, ASCE, Reston, VA, 1998, pp. 144–154.*
- [87] H.A. Toutanji, T. El-Korchi, in: *Proceedings of the International Seminar on Repair and Rehabilitation of Reinforced Concrete Structures: The State of the Art, ASCE, Reston, VA, 1998, pp. 134–143.*
- [88] Z. Geng, M.J. Chajes, T. Chou, D.Y. Pan, *Compos. Sci. Technol.* 58 (8) (1998) 1297–1305.
- [89] I. Gergely, C.P. Pantelides, R.J. Nuismer, L.D. Reaveley, *J. Compos. Construction* 2 (4) (1998) 165–174.
- [90] H.N. Garden, L.C. Hollaway, *Composites B* 29 (4) (1998) 411–424.
- [91] K. Kikukawa, K. Mutoh, H. Ohya, Y. Ohyama, H. Tanaka, K. Watanabe, *Compos. Interfaces* 5 (5) (1998) 469–478.
- [92] M. Xie, V.M. Karbhari, *J. Compos. Mater.* 32 (21) (1998) 1894–1913.
- [93] V.M. Karbhari, M. Engineer, D.A. Eckel II, *J. Mater. Sci.* 32 (1) (1997) 147–156.
- [94] D.P. Henkel, J.D. Wood, *NDT Int.* 24 (5) (1991) 259–264.
- [95] A.K. Pandey, M. Biswas, *J. Sound Vib.* 169 (1) (1994) 3–17.
- [96] Z. Mei, D.D.L. Chung, *Cem. Concr. Res.* 30 (5) (2000) 799–802.
- [97] H. Marzouk, D. Jiang, *ACI Mater. J.* 91 (6) (1994) 577–586.
- [98] L. Biolzi, G.L. Guerrini, G. Rosati, *J. Mater. Civil Eng.* 11 (2) (1999) 167–170.
- [99] J.H. Rutherford, B.W. Langan, M.A. Ward, *Cem. Concr. Aggregates* 16 (1) (1994) 78–82.
- [100] D. Bordeleau, M. Pigeon, N. Banthia, *ACI Mater. J.* 89 (6) (1992) 547–553.
- [101] B.B. Sabir, *Cem. Concr. Compos.* 19 (4) (1997) 285–294.
- [102] H. Mori, Y. Ishikawa, T. Shibata, T. Okamoto, *Zairyo (J. Soc. Mater. Sci. Jpn.)* 48 (8) (1999) 889–894.
- [103] T. Bakharev, L.J. Struble, in: *Proceedings of the 1994 MRS Fall Meeting on Microstructure of Cement-Based Systems/Bonding and Interfaces in Cementitious Materials, vol. 370, Materials Research Society, Pittsburgh, PA, 1995, pp. 83–88.*

- [104] N.M. Akhras, *Cem. Concr. Res.* 28 (9) (1998) 1275–1280.
- [105] H. Cai, X. Liu, *Cem. Concr. Res.* 28 (9) (1998) 1281–1287.
- [106] S. Wen, D.D.L. Chung, *Cem. Concr. Res.* 29 (6) (1999) 961–965.
- [107] J. Cao, D.D.L. Chung, *Cem. Concr. Res.* 32 (10) (2002) 1657–1661.
- [108] S.K. Kaushik, V.P. Bhargava, V. Kumar, *Indian Concr. J.* 75 (8) (2001) 515–521.
- [109] J. Li, Y. Yao, *Cem. Concr. Res.* 31 (8) (2001) 1203–1206.
- [110] V. Sicard, R. Francois, E. Ringot, G. Pons, *Cem. Concr. Res.* 22 (1) (1992) 159–168.
- [111] Y. Ishikawa, H. Kikukawa, T. Tanabe, *Trans. Jpn. Concr. Inst.* 18 (1996) 107–114.
- [112] G. De Schutter, L. Taerwe, *Mater. Struct.* 33 (230) (2000) 370–380.
- [113] K. Kovler, *J. Mater. Civil Eng.* 11 (1) (1999) 84–87.
- [114] G. De Schutter, L. Taerwe, *Mag. Concr. Res.* 49 (180) (1997) 195–200.
- [115] A.A. Khan, W.D. Cook, D. Mitchell, *ACI Mater. J.* 94 (2) (1997) 156–163.
- [116] Z. Li, *Int. J. Fract.* 66 (2) (1994) 189–196.
- [117] A.S. Ngab, A.H. Nilson, F.O. Slate, *J. Am. Concr. Inst.* 78 (4) (1981) 255–261.
- [118] M.M. Smadi, F.O. Slate, *ACI Mater. J.* 86 (2) (1989) 117–127.
- [119] Z.P. Bazant, J.-K. Kim, *Mater. Struct.* 24 (144) (1991) 409–421.
- [120] R.N. Swamy, G.H. Lambert, in: *Proceedings of the Second International Conference*, vol. 1, Publication SP 91, American Concrete Institute, Detroit, MI, 1991, pp. 145–170.
- [121] F. Furumura, T. Ave, W.J. Kim, *Report of the Research Laboratory of Engineering Materials*, vol. 11, Tokyo Institute of Technology, 1986, pp. 183–199.
- [122] S. Ohgishi, M. Wada, H. Ono, in: *Proceedings of the Symposium on Computer Networking*, vol. 3, Pergamon Press, Oxford, UK, 1980, pp. 109–119.
- [123] S.G. Reid, C. Qin, in: *Proceedings of the Second National Structural Engineering Conference*, vol. 90, part 10, National Conference Publication, Institution of Engineers, Barton, Australia, 1990, pp. 255–258.
- [124] H. Gao, G. Liu, F. Chen, *Qinghua Daxue Xuebao (J. Tsinghua Univ.)* 41 (11) (2001) 110–113.
- [125] E.A. Kogan, *Gidrotekhnicheskoe Stroitel’Stvo (Hydrotech. Construction)* 17 (9) (1983) 448–452.
- [126] J.L. Clement, F. Le Maou, *Bull. de Liaison des Laboratoires des Ponts et Chaussees* 228 (1993) 333–339.
- [127] A. Benaissa, P. Morlier, C. Viguier, *Mater. Struct.* 26 (160) (1993) 333–339.
- [128] E.K. Attiogbe, D. Darwin, *ACI Mater. J.* 85 (1) (1988) 3–11.
- [129] J. Zhu, L. Chen, X. Yan, *Gong Cheng Li Xue (Eng. Mech.)* 15 (3) (1998) 111–117.
- [130] S. Ghosh, K.W. Nasser, *Can. J. Civil Eng.* 22 (3) (1995) 621–636.
- [131] K. Wiegink, S. Marikunte, S.P. Shah, *ACI Mater. J.* 93 (5) (1996) 409–415.
- [132] R.P. Khatrri, V. Sirivivatnanon, W. Gross, *Cem. Concr. Res.* 25 (1) (1995) 209–220.
- [133] W.A. Al-Khaja, *Construction Building Mater.* 8 (3) (1994) 169–172.
- [134] R.S. Ghosh, J. Timusk, *J. Am. Concr. Inst.* 78 (5) (1981) 351–357.
- [135] P.S. Mangat, A.M. Motamedi, *Mater. Struct.* 113 (1986) 361–370.
- [136] P.S. Mangat, M.M. Azari, *J. Mater. Sci.* 20 (3) (1985) 1119–1133.
- [137] J. Cao, D.D.L. Chung, *Cem. Concr. Res.*, in press.
- [138] V. Baroghel-Bouny, J. Godin, *Bull. de Liaison des Laboratoires des Ponts et Chaussees* 218 (1998) 39–48.
- [139] M.D. Luther, P.A. Smith, in: *Proceedings of the Conference of the Engineering Foundation*, 1991, pp. 75–106.
- [140] V.M. Malhotra, *Concr. Int.: Des. Construction* 15 (4) (1993) 23–28.
- [141] M.D. Luther, *Concr. Int.: Des. Construction* 15 (4) (1993) 29–33.
- [142] J. Wolsiefer, D.R. Morgan, *Concr. Int.: Des. Construction* 15 (4) (1993) 34–39.
- [143] D.D.L. Chung, *J. Mater. Sci.* 37 (4) (2002) 673–682.
- [144] Y. Xu, D.D.L. Chung, *Cem. Concr. Res.* 30 (8) (2000) 1305–1311.
- [145] M.N. Haque, *Cem. Concr. Compos.* 18 (5) (1996) 333–342.
- [146] S.H. Alsayed, *Cem. Concr. Res.* 28 (10) (1998) 1405–1415.
- [147] A. Lamontagne, M. Pigeon, R. Pleau, D. Beaupre, *ACI Mater. J.* 93 (1) (1996) 69–74.
- [148] M.G. Alexander, *Adv. Cem. Res.* 6 (22) (1994) 73–81.
- [149] F.H. Al-Sugair, *Mag. Concr. Res.* 47 (170) (1995) 77–81.
- [150] B. Bissonnette, M. Pigeon, *Cem. Concr. Res.* 25 (5) (1995) 1075–1085.
- [151] G.A. Rao, *Cem. Concr. Res.* 28 (10) (1998) 1505–1509.
- [152] Z. Li, M. Qi, Z. Li, B. Ma, *J. Mater. Civil Eng.* 11 (3) (1999) 214–223.
- [153] O.M. Jensen, P.F. Hansen, *ACI Mater. J.* 93 (6) (1996) 539–543.
- [154] O.M. Jensen, P.F. Hansen, *Adv. Cem. Res.* 7 (25) (1995) 33–38.
- [155] P.-W. Chen, D.D.L. Chung, *Composites* 24 (1) (1993) 33–52.
- [156] J. Cao, D.D.L. Chung, *Cem. Concr. Res.*, in press.